On Bragg resonances and wave triad interactions in two-layered shear flows

Raunak Raj[1] and Anirban Guha[1,†]

[1]Environmental and Geophysical Fluids Group, Department of Mechanical Engineering,
Indian Institute of Technology, Kanpur, U.P. 208016, India

The standard resonance conditions for Bragg scattering as well as weakly nonlinear wave triads have been traditionally derived in the absence of any background velocity. In this paper, we have studied how these resonance conditions get modified when uniform, as well as various piecewise linear velocity profiles, are considered for two-layered shear flows. Background velocity can influence the resonance conditions in two ways: (i) by causing Doppler shifts, and (ii) by changing the intrinsic frequencies of the waves. For Bragg resonance, even a uniform velocity field changes the resonance condition. Velocity shear strongly influences the resonance conditions since, in addition to changing the intrinsic frequencies, it can cause unequal Doppler shifts between the surface, pycnocline and the bottom. Using multiple scale analysis and Fredholm alternative, we analytically obtain the equations governing both the Bragg resonance and the wave triads. We have also extended the higher-order spectral method, a highly efficient computational tool usually used to study triad and Bragg resonance problems, to incorporate the effect of piecewise linear velocity profile. A significant aspect, both on the theoretical and numerical fronts, has been extending the potential flow approximation, which is the basis of the study of these kinds of problems, to incorporate piecewise constant background shear.

Key words: coastal engineering, nonlinear instability, stratified flows

1. Introduction

'Wave triad interaction', the nonlinear interaction between three waves (or modes) satisfying a certain resonant condition, is a fundamental mechanism of energy transfer in fluid flows due to the nonlinear nature of the governing Navier–Stokes equations. In a two-layered density stratified flow in the absence of background velocity, Ball (1964) showed that two counter-propagating surface gravity waves can give rise to an interfacial gravity wave by forming a wave triad. Although Ball had ruled out the possibility of the existence of any other triads involving two surface modes, such interactions were later observed between three co-propagating modes – two surface waves and one interfacial wave (Baker, Meiron & Orszag 1982). In fact, two counter-propagating interfacial gravity waves can also give rise to a surface gravity wave (Wen 1995; Hill & Foda 1996). Remarkably enough, a rippled bottom

† Email address for correspondence: anirbanguha.ubc@gmail.com

topography can act like a neutral, stationary wave and mediate nonlinear energy transfer between two waves – a phenomenon known as the 'Bragg resonance' (Davies 1982; Mei 1985; Kirby 1986). Bragg resonance strongly affects the wave spectrum in continental shelves and coastal regions (Ball 1964), and also modifies the shore-parallel sandbars (Heathershaw & Davies 1985; Elgar, Raubenheimer & Herbers 2003). A study of Bragg resonance was performed in a two-layered density stratified flow by Alam, Liu & Yue (2009a). They showed that second-order nonlinearity may cause a surface wave propagating over a rippled bottom to transfer energy to (i) an interfacial wave propagating in the same direction (of the surface wave), (ii) an interfacial wave propagating in the opposite direction or (iii) a surface wave propagating in the same direction, depending on the wavenumber of the bottom ripple. Similar results were also obtained for an interfacial wave. Alam *et al.* (2009a) also studied interactions up to the third order of nonlinearity, thereby giving rise to various classes of Bragg resonance. The numerical simulations for the same were performed using a higher-order spectral (HOS) code (Alam, Liu & Yue 2009b), which was initially developed for a single-layered flow over bottom topography by Dommermuth & Yue (1987). Although the equations governing a single triad can also be analytically obtained without much difficulty up to the second order of nonlinearity, numerical simulation allows one to incorporate multiple triads up to several orders of nonlinearity. In most of the above-mentioned analytical and numerical (e.g. HOS) studies on wave triads or Bragg resonances, the base velocity was assumed to be absent. This is because these analytical and numerical treatments were based on the potential flow theory. The primary advantage of using the potential flow assumption is that it leads to an outstanding simplification – one can solve for the interfaces only. This allows a deeper insight into the complex nonlinear problem of resonant triad interactions and subsequent energy transfer. A general base flow falls beyond the purview of the potential flow theory, and in such flows the dynamics doesn't remain confined at the interfaces.

Since atmospheric and oceanic flows usually have base velocities (Vallis 2017), application of the 'standard' potential flow theory to such flows may be an over-simplification. Furthermore, The velocity present in the ocean, especially in the littoral region and estuaries, can be substantial (Geyer, Ralston & Holleman 2017). Further, it is also well known that the shear can affect the dynamics of the problem (Peregrine 1976). In order to accommodate shear in the study of wave triad interaction, in this work, we have considered a two-layered density stratified flow in the presence of a piecewise linear base velocity profile (or in other words, piecewise constant shear profile). While piecewise profiles similar to the ones we have considered here have been widely studied in the context of linear instabilities (Drazin 2002; Vallis 2017), studies involving nonlinear waves and instabilities in the presence of piecewise constant shear are very limited. We have shown that such a kind of velocity profile can be included under the umbrella of the extended potential flow theory (Guha & Raj 2018). Therefore, the dynamics is still localised at the interfaces, even though there is a base velocity present. Piecewise linear base velocity implies that the base vorticity is layerwise constant. Here, no vorticity is generated in the perturbed flow except at the interfaces. In other words, if the initial disturbances are irrotational, the perturbed flow in the bulk remains irrotational forever, despite the fact that the base flow is vortical (Guha & Raj 2018). This fundamental concept has also allowed us to use and extend the general framework of the HOS method by incorporating a piecewise linear velocity profile. For the case of wave triad interaction, adding a constant base velocity does not change the dynamics of the problem because

all the frequencies are merely Doppler shifted. It can also be intuitively seen that adding a uniform flow 'U' is similar to moving in a reference frame with a velocity 'U', and change of the reference frame should not change the dynamics of a problem. Any non-trivial base velocity profile, however, will break the otherwise symmetric nature of the dispersion relation of surface/interfacial gravity waves. On the other hand, addition of a constant base velocity leads to a significant alteration in the resonance conditions for Bragg resonance (Kirby 1988); here, the Doppler shift is not simply equivalent to changing of the reference frame because of the involvement of the bottom topography. The fact that the bottom topography is at rest while the surface and the interface have some base flow results in an unequal Doppler shift between the surface/interface and the bottom topography.

Significant changes occur when a uniform shear is present in each layer. When there is a jump in the base vorticity (i.e. shear) across an interface, it leads to vorticity waves. In addition, if there is a buoyancy jump at the same interface, we get vorticity–gravity waves (Harnik *et al.* 2008). Interaction between an interfacial vorticity wave (with no buoyancy jump) and a surface gravity wave was the focus of a recent study by Drivas & Wunsch (2016). Due to the presence of shear, the surface and the interface move with different base velocities, which significantly alters the conditions for the formation of resonant triads. Therefore, we expect that the problems involving triad interactions and Bragg resonances are remarkably enriched when a piecewise linear base velocity field is present.

The paper is organised as follows. In §2, we have shown the applicability of potential flow theory to piecewise linear velocity profiles. Furthermore, we have derived the modified evolution equations, which have been subsequently applied to the HOS code in order to incorporate the velocity field. We also use the evolution equations to obtain the dispersion relation of a general two-layered flow with a velocity field. This is followed by a perturbation expansion of the variables till $O(\epsilon^2)$, and using the Fredholm alternative, we obtain the analytical solution for amplitude variation both for the case of Bragg resonance and wave triad interaction. Here, the expansion parameter ϵ measures the steepness of the wave and following Alam *et al.* (2009b), we assume the steepness of the wave and the bottom to be of the same order. In §3, we have explored the effect of different types of velocity fields on different types of Bragg resonance triad using dispersion relations. In §4, we have briefly explained the effect of velocity field on wave triad interactions. We have devoted §5 to the numerical code and simulation. In this section, we have described the HOS code, which we have extended to incorporate piecewise linear velocity profiles. After validating the code, we have shown some numerical simulations to corroborate our analytical derivations. Finally, we summarise and conclude the paper in §6.

2. Theory

The kinematic boundary conditions and the dynamic boundary conditions for the water wave problem are nonlinear, suggesting that waves can interchange energy between them through a nonlinear interaction. This nonlinear exchange of energy between the waves, known as the wave triad interaction, is maximum when the waves involved satisfy a specific resonance condition. Although the energy exchange is a weakly nonlinear phenomenon, the condition for triad interactions can simply be obtained from the linear dispersion relations. The condition for the resonance between waves of wavenumbers (k_1, k_2 and k_3) and frequencies (ω_1, ω_2 and ω_3) is

$$k_3 = k_1 \pm k_2, \tag{2.1a}$$
$$\omega_3 = \omega_1 \pm \omega_2. \tag{2.1b}$$

The above condition basically means that if on the k–ω plane, waves are denoted by the vectors (k_1, ω_1), (k_2, ω_2) and (k_3, ω_3), then one of the vectors is equal to the sum of the other two (Ball 1964). Further, when two waves exchange energy with each other via mediation of the bottom ripples, which acts as a stationary wave with zero frequency, it is known as the Bragg resonance. Here, the resonance condition becomes

$$k_2 = k_1 \pm k_b, \qquad (2.2a)$$
$$\omega_1 = \omega_2. \qquad (2.2b)$$

For the case of no velocity, the dispersion relation is a biquadratic polynomial in ω, and is given as (Ball 1964; Alam *et al.* 2009*a*)

$$\omega^4(R + \coth kh_u \coth kh_l) - \omega^2 gk(\coth kh_u + \coth kh_l) + g^2 k^2 (1 - R) = 0. \qquad (2.3)$$

Here $R \equiv \rho_u/\rho_l$ is the density ratio, and h_u and h_l are respectively the depths of the upper and lower layers. Throughout the paper, the subscripts u and l respectively denote 'upper' and 'lower'. The implication of (2.3) being a biquadratic in ω is that the leftward travelling waves and the rightward travelling waves are symmetric, i.e. the difference between the two is simply a matter of a change in the sign of ω. However, in the presence of a uniform velocity U, the intrinsic frequencies of the waves are Doppler shifted by an amount 'Uk'. Further, if the velocity field is a function of the vertical coordinate 'z', then a vorticity wave may also be present, which will alter the intrinsic frequency of the waves as well, and the biquadratic and symmetric nature of the dispersion relation will be lost. We have classified the velocity profiles into four categories: (i) a uniform flow, (ii) shear only in the lower layer, (iii) shear only in the upper layer, (iv) shear in both the layers. These cases are shown in figure 1. In the first case, the surface and the interface are not Doppler shifted with respect to each other but they are Doppler shifted with respect to the bottom. This should mean that the condition for wave triad interaction will not change but the condition for Bragg resonance should be altered. Further, there will not be any change in the intrinsic frequencies of any of the waves present in the system. In the second case, shear is only present in the lower layer. This case is similar to the first one with reference to the Doppler shifts, i.e. both the surface, and the interface between ρ_u and ρ_l (hereafter, simply referred to as 'interface' or 'pycnocline'), are Doppler shifted equally with respect to the bottom, but additionally, the intrinsic frequencies of the waves will change due to the presence of a shear jump at the interface. In the third case, shear is present only in the upper layer and hence the surface and the interface are Doppler shifted; moreover, there is a shear jump present at the interface too. Hence, the intrinsic frequencies of the waves will also change. In the last case, shear is present in both layers. Hence, there is a shear jump both at the interface and at the surface and the surface and the interface are Doppler shifted unequally with respect to the bottom. It is also to be noted here that the velocity difference between the surface and the interface, i.e. the second and the fourth cases, might lead to linear instabilities as well due to the formation of a counter-propagating system (Guha & Lawrence 2014; Shete & Guha 2018). However, such linear instabilities, for moderate values of shear, are restricted to high wavenumbers and do not have appreciable growth rates. In any case, we would be focussing on the nonlinear interactions only.

It was shown in Guha & Raj (2018) that, in the presence of a piecewise linear velocity profile, there is no perturbation vorticity generation in the fluid bulk and
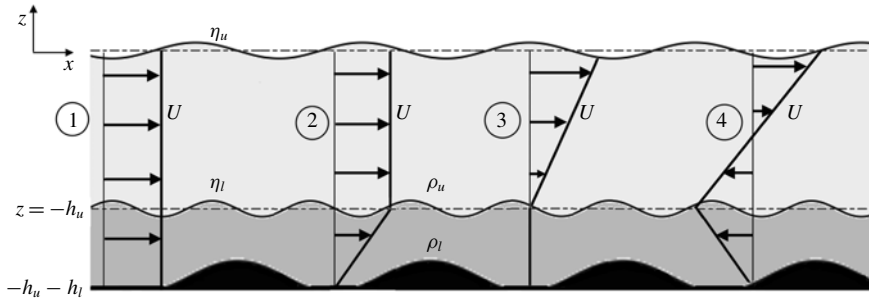
FIGURE 1. Schematic of a two-layered density stratified flow in the presence of a bottom topography and various kinds of simple velocity profiles, labelled by ①: uniform flow, ②: constant shear in the bottom layer, ③: constant shear in the top layer and ④: constant shear in both layers.

vorticity is generated exclusively at the interfaces. This means that if the bulk flow is initially irrotational, then it will remain so forever, similar to the scenario of no background velocity. Further, if there is a density difference (ρ_1, ρ_2) as well a shear difference (Ω_1, Ω_2) across any general (hence subscripts '1' and '2' are used, instead of 'u' and 'l') interface $z = h_0 + \eta(x, t)$ moving in a velocity field $U = U(z)$, then the dynamic boundary condition at any interface $z = h_0 + \eta(x, t)$ is given by (see appendix A for derivation)

$$\rho_1 \left[\phi_{1,t} + \tfrac{1}{2}(\phi_{1,x}^2 + \phi_{1,z}^2) + U\phi_{1,x} - \Omega_1\psi_1 + g\eta \right]$$
$$= \rho_2 \left[\phi_{2,t} + \tfrac{1}{2}(\phi_{2,x}^2 + \phi_{2,z}^2) + U\phi_{2,x} - \Omega_2\psi_2 + g\eta \right]. \quad (2.4)$$

Here, ϕ_1 and ϕ_2 are respectively the perturbation velocity potentials of fluids '1' and '2', while ψ_1 and ψ_2 are the same for the streamfunctions, which can be obtained using the respective velocity potentials. The comma in the subscript denotes partial derivative; for example, $\eta_{1,x} \equiv \partial\eta_1/\partial x$. In the above equation, the terms $U\phi_{1,x}$ and $U\phi_{2,x}$ are the 'Doppler shift' terms indicating that the interface is moving in a velocity field U. The terms $\Omega_1\psi_1$ and $\Omega_2\psi_2$ appear due to the presence of the constant shears Ω_1 and Ω_2 on either side of the interface. Rest all other terms are usual and appear in the absence of velocity as well. Similarly, the kinematic boundary condition for the same interface will be given by

$$\eta_{,t} + (U + \phi_{,x})\eta_{,x} = \phi_{,z}. \quad (2.5)$$

Here, the term $U\eta_{,x}$ is the Doppler shift term. We will apply both kinematic and dynamic boundary conditions to the surface and the interface in figure 1. The above equations are applicable at the interface i.e. at $z = h_0 + \eta(x, t)$. More accurately, the left-hand side of the dynamic boundary condition is evaluated just above the interface $z = h_0 + \eta(x, t)$ whereas, the right-hand side is evaluated just below the interface. On the other hand, for the kinematic boundary condition, there are two separate equations – one above the interface and one below it. However, quite often in this paper, we will use the Taylor expansion to evaluate the variables at the mean level i.e. $z = h_0$. In particular, the velocity $U(z)$ just above the interface would be given as

$$U = U_0 + \Omega_1\eta, \quad (2.6)$$

and just below the interface it will be

$$U = U_0 + \Omega_2 \eta, \qquad (2.7)$$

where $U_0 = U(h_0)$.

2.1. *Framework*

Here we give a general framework that consists of a system of equations at $O(\epsilon)$ and $O(\epsilon^2)$, which is obtained using perturbation analysis and the method of multiple scales for a periodic wave train. We have kept the system quite general so as to use the system of equations for the purpose of wave triad interaction (see § 2.2) and Bragg resonance (see § 2.3).

We consider a two-interface system with piecewise constant density and vorticity in each layer, see figure 1. The velocity profile is continuous, but the derivative of velocity may have a discontinuity at the density interface. The total depth of the system is H and $H = h_u + h_l$. The fluid above the surface is assumed to be a zero density fluid and R is the density ratio at the interface ($R \equiv \rho_u/\rho_l$). The base velocity profile is piecewise linear, and has the values $U = \{U_u, U_l, U_b\}$ at $z = \{0, -h_u, -h_u - h_l\}$ respectively. The vertical (z) axis points upwards, hence the gravity (g) is along the negative z-direction. The elevations of the surface and the pycnocline from their respective mean levels are $\eta_u(x, t)$ and $\eta_l(x, t)$. Similarly, the elevation of the bottom topography is $\eta_b(x)$ from its mean level at $z = -h_u - h_l$. As mentioned already, for a piecewise linear base velocity profile perturbed by irrotational initial disturbances, the vorticity generation is limited to the interfaces and the bulk flow remains irrotational. This allows us to introduce the velocity potentials ϕ_u and ϕ_l respectively in the upper and the lower layers. Hence, the continuity equation reduces to the Laplace equation

$$\nabla^2 \phi_u = 0 \quad -h_u + \eta_l < z < \eta_u, \qquad (2.8a)$$

$$\nabla^2 \phi_l = 0 \quad -h_u - h_l + \eta_b < z < -h_u + \eta_l. \qquad (2.8b)$$

The kinematic boundary conditions are

$$\eta_{u,t} + (U + \phi_{u,x})\eta_{u,x} = \phi_{u,z} \quad \text{at } z = \eta_u, \qquad (2.9a)$$

$$\eta_{l,t} + (U + \phi_{u,x})\eta_{l,x} = \phi_{u,z} \quad \text{at } z = -h_u + \eta_l, \qquad (2.9b)$$

$$\eta_{l,t} + (U + \phi_{l,x})\eta_{l,x} = \phi_{l,z} \quad \text{at } z = -h_u + \eta_l, \qquad (2.9c)$$

$$(U + \phi_{l,x})\eta_{b,x} = \phi_{l,z} \quad \text{at } z = -h_u - h_l + \eta_b. \qquad (2.9d)$$

Likewise, the dynamic boundary conditions are as follows:

$$\phi_{u,t} + \tfrac{1}{2}(\phi_{u,x}^2 + \phi_{u,z}^2) + U\phi_{u,x} - \Omega_u \psi_u + g\eta_u = 0 \quad \text{at } z = \eta_u, \qquad (2.9e)$$

$$\rho_u \left[\phi_{u,t} + \tfrac{1}{2}(\phi_{u,x}^2 + \phi_{u,z}^2) + U\phi_{u,x} - \Omega_u \psi_u + g\eta_l \right]$$
$$- \rho_l \left[\phi_{l,t} + \tfrac{1}{2}(\phi_{l,x}^2 + \phi_{l,z}^2) + U\phi_{l,x} - \Omega_l \psi_l + g\eta_l \right] = 0 \quad \text{at } z = -h_u + \eta_l. \qquad (2.9f)$$

We are interested in obtaining the solutions up to the first order of nonlinearity. Hence, we perform a perturbation expansion until $O(\epsilon^2)$, where the expansion

parameter ϵ measures the wave steepness. It is also assumed that the steepness of the bottom topography is $O(\epsilon)$.

$$\phi_u(x, z, t) = \epsilon\phi_u^{(1)}(x, z, t, \tau) + \epsilon^2\phi_u^{(2)}(x, z, t, \tau), \quad (2.10a)$$

$$\phi_l(x, z, t) = \epsilon\phi_l^{(1)}(x, z, t, \tau) + \epsilon^2\phi_l^{(2)}(x, z, t, \tau), \quad (2.10b)$$

$$\eta_u(x, t) = \epsilon\eta_u^{(1)}(x, t, \tau) + \epsilon^2\eta_u^{(2)}(x, t, \tau), \quad (2.10c)$$

$$\eta_l(x, t) = \epsilon\eta_l^{(1)}(x, t, \tau) + \epsilon^2\eta_l^{(2)}(x, t, \tau). \quad (2.10d)$$

Here we have assumed that the potentials and elevations have a slow time scale 'τ' associated with them such that $\tau = \epsilon t$. The superscripts (1) and (2) respectively denote the $O(\epsilon)$ and $O(\epsilon^2)$ terms. Further, we expand the velocity potential ϕ and the streamfunction ψ in a Taylor series about the respective mean surface/interface, which at $O(\epsilon)$ gives the following set of equations:

$$\phi_{u,z}^{(1)} - \eta_{u,t}^{(1)} - U_u\eta_{u,x}^{(1)} = 0 \quad \text{at } z = 0, \quad (2.11a)$$

$$\phi_{u,z}^{(1)} - \eta_{l,t}^{(1)} - U_l\eta_{l,x}^{(1)} = 0 \quad \text{at } z = -h_u, \quad (2.11b)$$

$$\phi_{l,z}^{(1)} - \eta_{l,t}^{(1)} - U_l\eta_{l,x}^{(1)} = 0 \quad \text{at } z = -h_u, \quad (2.11c)$$

$$\phi_{u,t}^{(1)} + U_u\phi_{u,x}^{(1)} - \Omega_u\psi_u^{(1)} + g\eta_u^{(1)} = 0 \quad \text{at } z = 0, \quad (2.11d)$$

$$R[\phi_{u,t}^{(1)} + U_l\phi_{u,x}^{(1)} - \Omega_u\psi_u^{(1)} + g\eta_l^{(1)}] \quad (2.11e)$$

$$-[\phi_{l,t}^{(1)} + U_l\phi_{l,x}^{(1)} - \Omega_l\psi_l^{(1)} + g\eta_l^{(1)}] = 0 \quad \text{at } z = -h_u, \quad (2.11f)$$

$$\phi_{l,z}^{(1)} = 0 \quad \text{at } z = -h_u - h_l. \quad (2.11g)$$

Additionally, we use the eigenfunction expansions with slowly varying amplitudes satisfying the respective Laplace equations. Thus for $j = \{1, 2, \ldots\}$ and $m = \{1, 2\}$, where the subscript j denotes the jth wavenumber and the superscript (m) denotes the order of nonlinearity, we get

$$\phi_{uj}^{(m)} = \left[A_j^{(m)}(\tau)\frac{\cosh k_j(z + h_u)}{\cosh(k_jh_u)} + B_j^{(m)}(\tau)\frac{\sinh k_jz}{\cosh(k_jh_u)}\right]e^{i(k_jx-\omega_jt)} + \text{c.c.}, \quad (2.12a)$$

$$\phi_{lj}^{(m)} = \left[C_j^{(m)}(\tau)\frac{\cosh k_j(z + h_u + h_l)}{\cosh(k_jh_l)} + D_j^{(m)}(\tau)\frac{\sinh k_j(z + h_u + h_l)}{\cosh(k_jh_l)}\right]e^{i(k_jx-\omega_jt)} + \text{c.c.}, \quad (2.12b)$$

$$\psi_{uj}^{(m)} = i\left[A_j^{(m)}(\tau)\frac{\sinh k_j(z + h_u)}{\cosh(k_jh_u)} + B_j^{(m)}(\tau)\frac{\cosh k_jz}{\cosh(k_jh_u)}\right]e^{i(k_jx-\omega_jt)} + \text{c.c.}, \quad (2.12c)$$

$$\psi_{lj}^{(m)} = i\left[C_j^{(m)}(\tau)\frac{\sinh k_j(z + h_u + h_l)}{\cosh(k_jh_l)} + D_j^{(m)}(\tau)\frac{\cosh k_j(z + h_u + h_l)}{\cosh(k_jh_l)}\right]e^{i(k_jx-\omega_jt)} + \text{c.c.}, \quad (2.12d)$$

$$\eta_{uj}^{(m)} = a_j^{(m)}(\tau)e^{i(k_jx-\omega_jt)} + \text{c.c.}, \quad (2.12e)$$

$$\eta_{lj}^{(m)} = b_j^{(m)}(\tau)e^{i(k_jx-\omega_jt)} + \text{c.c.}, \quad (2.12f)$$

where c.c. denotes complex conjugate. Substituting the above equations (2.12a)–(2.12f) in (2.11a)–(2.11g) at $O(\epsilon)$, we obtain a set of linear equations corresponding to any given wavenumber k_j at $O(\epsilon)$, the homogeneous part of which is

$$\mathbf{D}(\omega_j, k_j)\mathbf{x}_j^{(1)} = 0. \quad (2.13)$$

Here, the vector $\boldsymbol{x}_j^{(1)} \equiv [A_j^{(1)}, B_j^{(1)}, C_j^{(1)}, D_j^{(1)}, a_j^{(1)}, b_j^{(1)}]^\dagger$, and the matrix $\boldsymbol{D}(\omega_j, k_j)$ is given by

$$
\begin{bmatrix}
\dfrac{k_j}{\coth(k_j h_u)} & \dfrac{k_j}{\cosh(k_j h_u)} & 0 & 0 & \mathrm{i}\omega_j^{\{1\}} & 0 \\[2ex]
0 & k_j & 0 & 0 & 0 & \mathrm{i}\omega_j^{\{2\}} \\[2ex]
0 & 0 & \dfrac{k_j}{\coth(k_j h_l)} & k & 0 & \mathrm{i}\omega_j^{(2)} \\[2ex]
-\mathrm{i}\omega_j^{(1)} - \dfrac{\mathrm{i}\Omega_u}{\coth(k_j h_u)} & -\dfrac{\mathrm{i}\Omega_u}{\cosh(k_j h_u)} & 0 & 0 & g & 0 \\[2ex]
-\dfrac{\mathrm{i}R\omega_j^{\{2\}}}{\cosh(k_j h_u)} & \dfrac{\mathrm{i}R\omega_j^{\{2\}}}{\coth(k_j h_u)} - \mathrm{i}R\Omega_u & \mathrm{i}\omega_j^{\{2\}} + \dfrac{\mathrm{i}\Omega_l}{\coth k_j h_l} & \dfrac{\mathrm{i}\omega_j^{(2)}}{\coth k_j h_l} + \mathrm{i}\Omega_l & 0 & g(R-1) \\[2ex]
0 & 0 & 0 & \dfrac{k_j}{\cosh k_j h_l} & 0 & 0
\end{bmatrix},
$$
$$(2.14)$$

where $\omega_j^{\{1\}} = \omega_j - U_u k_j$; $\omega_j^{\{2\}} = \omega_j - U_l k_j$. The dispersion relation of the above system is obtained by setting the determinant of the above matrix to zero and is given by the equation

$$\det(\boldsymbol{D})(\omega_j, k_j) = 0, \tag{2.15}$$

where $\det(\boldsymbol{D})(\omega_j, k_j)$ is the determinant of the matrix $\boldsymbol{D}(\omega_j, k_j)$.

In addition to the homogeneous solution, we also have the particular solutions at $O(\epsilon)$ due to the velocity difference between the bottom and the fluid above it. In such a case, the time-independent surface elevation, capturing the non-homogeneity introduced by the mean flow's interaction with the bottom, is given by

$$\hat{\eta}_u = -\frac{U_u U_b U_l^2 k_b^6}{\cosh(k_b h_u) \cosh^2(k_b h_l) \det(\boldsymbol{D})(0, k_b)} \hat{\eta}_b, \tag{2.16}$$

and other coefficients, i.e. $\hat{\eta}_l, A, B, C, D$ are given in appendix B.

At $O(\epsilon^2)$, we obtain the following equations:

$$\phi_{u,z}^{(2)} - \eta_{u,t}^{(2)} - U_u \eta_{u,x}^{(2)} = p_1 + q_1 \quad \text{at } z = 0, \tag{2.17a}$$

$$\phi_{u,z}^{(2)} - \eta_{l,t}^{(2)} - U_l \eta_{l,x}^{(2)} = p_2 + q_2 \quad \text{at } z = -h_u, \tag{2.17b}$$

$$\phi_{l,z}^{(2)} - \eta_{l,t}^{(2)} - U_l \eta_{l,x}^{(2)} = p_3 + q_3 \quad \text{at } z = -h_u, \tag{2.17c}$$

$$\phi_{u,t}^{(2)} + U_u \phi_{u,x}^{(2)} - \Omega_u \psi_u^{(2)} + g\eta_u^{(2)} = p_4 + q_4 \quad \text{at } z = 0, \tag{2.17d}$$

$$[\phi_{u,t}^{(2)} + U_l \phi_{u,x}^{(2)} - \Omega_u \psi_u^{(2)} + g\eta_l^{(2)}]$$
$$-[\phi_{l,t}^{(2)} + U_l \phi_{l,x}^{(2)} - \Omega_l \psi_l^{(2)} + g\eta_l^{(2)}] = p_5 + q_5 \quad \text{at } z = -h_u, \tag{2.17e}$$

$$\phi_{l,z}^{(2)} = p_6 + q_6 \quad \text{at } z = -h_u - h_l. \tag{2.17f}$$

The right-hand side terms p_1, p_2, p_3, p_4, p_5 and p_6 are the products of two $O(\epsilon)$ terms and for neatness, we have removed the superscript '(1)' from the variables. They are given as

$$p_1 = \eta_{u,x}(\phi_{u,x} + \Omega_u \eta_u) - \eta_u \phi_{u,zz} \quad z = 0, \tag{2.18a}$$

$$p_2 = \eta_{l,x}(\phi_{u,x} + \Omega_u \eta_l) - \eta_l \phi_{u,zz} \quad z = -h_u, \tag{2.18b}$$

$$p_3 = \eta_{l,x}(\phi_{l,x} + \Omega_l \eta_l) - \eta_l \phi_{l,zz} \quad z = -h_u, \tag{2.18c}$$

$$p_4 = -\eta_u(\phi_{u,tz} + U_u \phi_{u,xz} + \Omega_u \phi_{u,x}) - \tfrac{1}{2}\left[(\phi_{u,x})^2 + (\phi_{u,z})^2\right] + \Omega_u \eta_u \psi_{u,z} \quad z = 0, \tag{2.18d}$$

$$\begin{aligned} p_5 = {} & R\left[\eta_l(\phi_{u,tz} + U_l \phi_{u,xz} + \Omega_u \phi_{u,x}) - \tfrac{1}{2}\left[(\phi_{u,x})^2 + (\phi_{u,z})^2\right] + \Omega_u \eta_l \psi_{u,z}\right] \\ & - \left[\eta_l(\phi_{l,tz} + U_l \phi_{l,xz} + \Omega_l \phi_{l,x}) - \tfrac{1}{2}\left[(\phi_{l,x})^2 + (\phi_{l,z})^2\right] + \Omega_l \eta_l \psi_{l,z}\right] \quad z = -h_u, \end{aligned} \tag{2.18e}$$

$$p_6 = \eta_{b,x}(\phi_{l,x} + \Omega_l \eta_b) - \eta_b \phi_{l,zz} \quad z = -h_u - h_l. \tag{2.18f}$$

Here, the right-hand side terms comprise of terms due to nonlinearity of the boundary condition as well as due to Taylor expansion about the mean level. The right-hand side terms q_1, q_2, q_3, q_4, q_5 and q_6 are the time derivatives of the $O(\epsilon)$ terms:

$$q_1 = \eta_{u,\tau}, \tag{2.19a}$$

$$q_2 = \eta_{l,\tau}, \tag{2.19b}$$

$$q_3 = \eta_{l,\tau}, \tag{2.19c}$$

$$q_4 = -\phi_{u,\tau}, \tag{2.19d}$$

$$q_5 = -R\phi_{u,\tau} + \phi_{l,\tau}, \tag{2.19e}$$

$$q_6 = 0. \tag{2.19f}$$

The set of equations obtained to this point are very general and works both for the case of wave triad interaction and Bragg resonance. This is because until this point, we have not made any assumption on the wavenumbers present in the system or if those wavenumbers satisfy any particular resonance condition. Hence, we will be using the above framework to obtain the analytical solutions for wave triad interaction in § 2.2 as well as Bragg resonance in § 2.3.

2.2. *Analytical solution for wave triad interaction*

We assume that initially at $O(\epsilon)$, the system has only three wavenumbers $\{k_1, k_2, k_3\}$ and corresponding frequencies $\{\omega_1, \omega_2, \omega_3\}$, satisfying the resonance condition. Without any loss of generality, the resonance condition is given by $k_1 = k_2 + k_3$ and $\omega_1 = \omega_2 + \omega_3$. The surface elevation expressed as a sum of these three modes reads

$$\eta_u^{(1)}(x, t, \tau) = a_1^{(1)}(\tau)e^{i(k_1 x - \omega_1 t)} + a_2^{(1)}(\tau)e^{i(k_2 x - \omega_2 t)} + a_3^{(1)}(\tau)e^{i(k_3 x - \omega_3 t)} + \text{c.c.} \tag{2.20}$$

The other functions $\phi_u^{(1)}$, $\phi_l^{(1)}$, $\psi_u^{(1)}$, $\psi_l^{(1)}$ and $\eta_l^{(1)}$ can also be written in a similar fashion. Substituting this in the equations at $O(\epsilon)$, we would obtain the following set of linear equations:

$$\boldsymbol{D}(\omega_1, k_1)\boldsymbol{x}_1^{(1)} = 0; \quad \boldsymbol{D}(\omega_2, k_2)\boldsymbol{x}_2^{(1)} = 0; \quad \boldsymbol{D}(\omega_3, k_3)\boldsymbol{x}_3^{(1)} = 0. \tag{2.21a-c}$$

The vector $\boldsymbol{x}_j^{(1)} \equiv [A_j^{(1)}, B_j^{(1)}, C_j^{(1)}, D_j^{(1)}, a_j^{(1)}, b_j^{(1)}]^{\dagger}$ and the matrix $\boldsymbol{D}(\omega, k)$ are given in § 2.1. We further proceed to substitute (2.12a)–(2.12f) in (2.17a)–(2.17f) at $O(\epsilon^2)$. Here, the left-hand sides of the equations obtained at $O(\epsilon^2)$ are similar to those obtained at $O(\epsilon)$. On substitution, we collect the terms corresponding to each wavenumber k_1, k_2 and k_3 after using the resonance conditions $k_1 = k_2 + k_3$ and $\omega_1 = \omega_2 + \omega_3$. We obtain equations of the form

$$\boldsymbol{D}(\omega_1, k_1)\boldsymbol{x}_1^{(2)} = \boldsymbol{v}_1 a_2^{(1)} a_3^{(1)} + \boldsymbol{r}_1 a_{1,\tau}^{(1)}, \tag{2.22a}$$

$$\boldsymbol{D}(\omega_2, k_2)\boldsymbol{x}_2^{(2)} = \boldsymbol{v}_2 \bar{a}_3^{(1)} a_1^{(1)} + \boldsymbol{r}_2 a_{2,\tau}^{(1)}, \tag{2.22b}$$

$$\boldsymbol{D}(\omega_3, k_3)\boldsymbol{x}_3^{(2)} = \boldsymbol{v}_3 a_1^{(1)} \bar{a}_2^{(1)} + \boldsymbol{r}_3 a_{3,\tau}^{(1)}, \tag{2.22c}$$

where overbar denotes complex conjugate. The vector $\boldsymbol{x}_j^{(2)} \equiv [A_j^{(2)}, B_j^{(2)}, C_j^{(2)}, D_j^{(2)}, a_j^{(2)}, b_j^{(2)}]^\dagger$ and the terms of the vector $\boldsymbol{v}_j$ and $\boldsymbol{r}_j$ are given in appendix B. The vector $\boldsymbol{v}_j$ comes from the coefficient of $\exp[\mathrm{i}(k_j x - \omega_j t)]$ present in the product of two $O(\epsilon)$ terms. Similarly, the vector $\boldsymbol{r}_j$ comes from the time derivatives of $O(\epsilon)$ terms. It might be noted here that the product terms contain combinations of various terms such as $A_i^{(1)} a_j^{(1)}$, $B_i^{(1)} a_j^{(1)}$, $C_i^{(1)} C_j^{(1)}$ etc.; however, we have converted each of these products into the product $a_i^{(1)} a_j^{(1)}$, i.e. in terms of products of amplitude of surface elevation by using the null space of the respective matrix $\boldsymbol{D}(\omega_j, k_j)$. Similarly, the slow time derivatives are also converted in terms of the slow time derivative of the surface elevations, i.e. $a_{j,\tau}^{(1)}$.

Using the Fredholm alternative in the context of the sets of (2.21) and (2.22), we deduce that the solutions for $\boldsymbol{x}_i^{(2)}$ exist if and only if the vectors $\boldsymbol{v}_i$ are orthogonal to the null space of the transpose of the respective matrices $\boldsymbol{D}(\omega_j, k_j)$. Denoting the null space of the transpose of the matrix $\boldsymbol{D}(\omega_j, k_j)$ by $\boldsymbol{n}_j$, we finally get a set of three equations:

$$\boldsymbol{n}_1 \cdot (\boldsymbol{v}_1 a_2^{(1)} a_3^{(1)} + \boldsymbol{r}_1 a_{1,\tau}^{(1)}) = 0, \tag{2.23a}$$

$$\boldsymbol{n}_2 \cdot (\boldsymbol{v}_2 \bar{a}_3^{(1)} a_1^{(1)} + \boldsymbol{r}_2 a_{2,\tau}^{(1)}) = 0, \tag{2.23b}$$

$$\boldsymbol{n}_3 \cdot (\boldsymbol{v}_3 a_1^{(1)} \bar{a}_2^{(1)} + \boldsymbol{r}_3 a_{3,\tau}^{(1)}) = 0, \tag{2.23c}$$

which finally gets reduced to

$$a_{1,\tau}^{(1)} = \beta_1 a_2^{(1)} a_3^{(1)}; \quad a_{2,\tau}^{(1)} = \beta_2 \bar{a}_3^{(1)} a_1^{(1)}; \quad a_{3,\tau}^{(1)} = \beta_3 a_1^{(1)} \bar{a}_2^{(1)}, \tag{2.24a--c}$$

where

$$\beta_j = -\frac{\boldsymbol{n}_j \cdot \boldsymbol{v}_j}{\boldsymbol{n}_j \cdot \boldsymbol{r}_j}. \tag{2.25}$$

2.3. *Analytical solution for Bragg resonance*

The equations for the case of Bragg resonance can also be obtained using the same framework as in §2.2. However, in the case of Bragg resonance, only two propagating waves are involved, the third one is the bottom ripple. We assume the participating waves to have the wavenumbers $\{k_1, k_2\}$ with frequencies $\{\omega_1, \omega_2\}$ and the bottom to have wavenumber k_b. Substituting the normal modes, we get a set of linear equations at $O(\epsilon)$:

$$\boldsymbol{D}(\omega_1, k_1)\boldsymbol{x}_1^{(1)} = 0; \quad \boldsymbol{D}(\omega_2, k_2)\boldsymbol{x}_2^{(1)} = 0. \tag{2.26a,b}$$

Here the vector $\boldsymbol{x}_j^{(1)} \equiv [A_j^{(1)}, B_j^{(1)}, C_j^{(1)}, D_j^{(1)}, a_j^{(1)}, b_j^{(1)}]^\dagger$ and the matrix $\boldsymbol{D}(\omega, k)$ are the same as those in §2.2. We assume that at $O(\epsilon)$, the surface consists of only two modes, k_1 and k_2. Hence we write $\eta_u^{(1)}(x, t)$ as

$$\eta_u^{(1)}(x, t, \tau) = a_1^{(1)}(\tau)\mathrm{e}^{\mathrm{i}(k_1 x - \omega_1 t)} + a_2^{(1)}(\tau)\mathrm{e}^{\mathrm{i}(k_2 x - \omega_2 t)} + \text{c.c.}, \tag{2.27}$$

$$\eta_b(x) = a_b \mathrm{e}^{\mathrm{i}k_1 x} + \text{c.c.} \tag{2.28}$$

The other functions $\phi_u^{(1)}$, $\phi_l^{(1)}$, $\psi_u^{(1)}$, $\psi_l^{(1)}$ and $\eta_l^{(1)}$ containing the wavenumbers 'k_1' and 'k_2' can also be written similarly. Substituting this in the equations at $O(\epsilon)$, we obtain a set of linear equations

$$\boldsymbol{D}(\omega_1, k_1)\boldsymbol{x}_1^{(1)} = 0; \quad \boldsymbol{D}(\omega_2, k_2)\boldsymbol{x}_2^{(1)} = 0. \tag{2.29a,b}$$

The vector $\boldsymbol{x}_j^{(1)} \equiv [A_j^{(1)}, B_j^{(1)}, C_j^{(1)}, D_j^{(1)}, a_j^{(1)}, b_j^{(1)}]^\dagger$ and the matrix $\boldsymbol{D}(\omega, k)$ are the same as those in § 2.2. We further proceed to substitute (2.12a)–(2.12f) in (2.17a)–(2.17f) at $O(\epsilon^2)$. Assuming $k_1 + k_2 = k_b$ and $\omega_1 + \omega_2 = 0$, we obtain

$$\boldsymbol{D}(\omega_1, k_1)\boldsymbol{x}_1^{(2)} = \boldsymbol{v}_1 a_b \bar{a}_2^{(1)} + \boldsymbol{r}_1 a_{1,\tau}^{(1)}, \tag{2.30}$$

$$\boldsymbol{D}(\omega_2, k_2)\boldsymbol{x}_2^{(2)} = \boldsymbol{v}_2 a_b \bar{a}_1^{(1)} + \boldsymbol{r}_2 a_{2,\tau}^{(1)}. \tag{2.31}$$

Denoting the null space of the transpose of $\boldsymbol{D}(k_j, \omega_j)$ by $\boldsymbol{n}_j$ and using the Fredholm alternative, we get the following set of equations:

$$a_{1,\tau}^{(1)} = \beta_1 a_b \bar{a}_2^{(1)}; \quad a_{2,\tau}^{(1)} = \beta_2 a_b \bar{a}_1^{(1)}, \tag{2.32a,b}$$

where

$$\beta_j = -\frac{\boldsymbol{n}_j \cdot \boldsymbol{v}_j}{\boldsymbol{n}_j \cdot \boldsymbol{r}_j}. \tag{2.33}$$

Furthermore, when $k_1 - k_2 = k_b$ and $\omega_1 - \omega_2 = 0$, we get

$$a_{1,\tau}^{(1)} = \beta_1 a_b a_2^{(1)}; \quad a_{2,\tau}^{(1)} = \beta_2 \bar{a}_b a_1^{(1)}, \tag{2.34a,b}$$

in which β_j remains the same as before.

3. Bragg resonance in the presence of a velocity field

In a single-layered flow in the absence of a velocity field, there can be only one condition for Bragg resonance – when the wavenumber of the bottom is twice the wavenumber of the surface wave i.e. $k_b = 2k_s$. In such a case, an oppositely travelling surface mode having the same frequency as that of the incident wave is generated by the resonant forcing of the bottom. However, in a two-layered flow, several other resonant pairs are possible (Alam *et al.* 2009a). As mentioned previously, in the presence of a pycnocline, there exist four different modes of propagation – two oppositely travelling surface (or external) modes and two oppositely travelling interfacial (or internal) modes. Any of these modes, depending on the wavenumber of the bottom ripples, may resonate with any other mode in the system, subject to the fulfilment of the resonance conditions. In the absence of a velocity field, there is an inherent symmetry in the weakly nonlinear wave interaction owing to the symmetric (or biquadratic) nature of the dispersion relation. This means that if a rightward travelling surface mode of wavenumber k_i interacts with the bottom of wavenumber k_b to resonantly generate a leftward travelling interfacial mode of wavenumber k_r, then a leftward travelling surface mode of wavenumber k_i will also interact with the same bottom of wavenumber k_b to resonantly generate a rightward travelling interfacial mode of wavenumber k_r. In the presence of a velocity field, however, this 'right–left symmetry' of the interaction is destroyed.

The presence of a velocity field may also change the intrinsic frequency of the waves. It may also cause a relative Doppler shift between the interfaces. When there
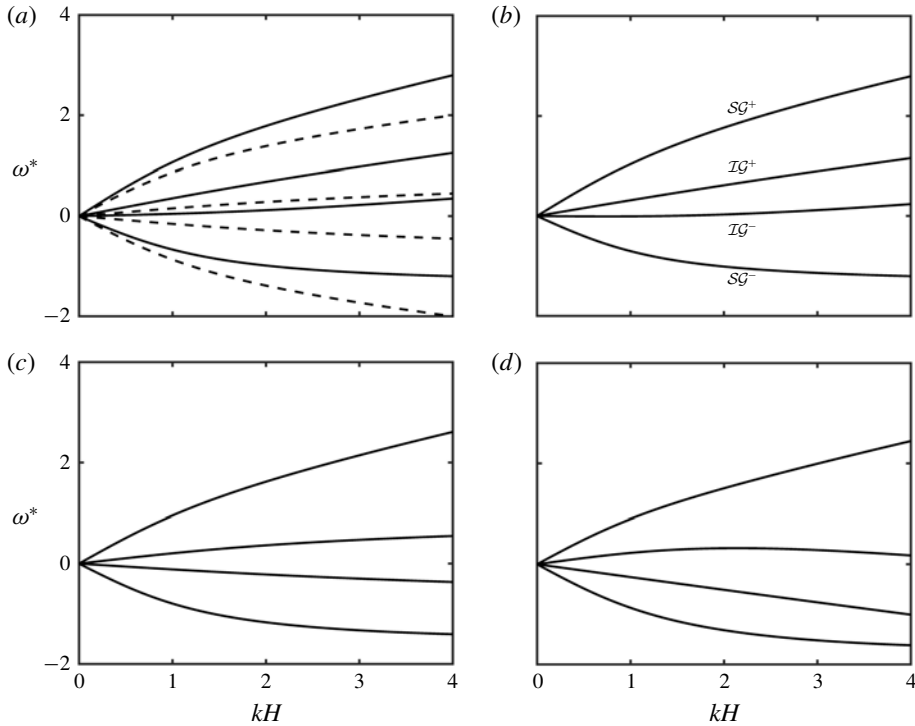
FIGURE 2. Dispersion relation for various velocity profiles with $h_u/h_l = 1$ and $R = 0.90$. (a) $U_u^* = U_l^* = U_b^* = 0.2$, (b) $U_u^* = U_l^* = 0.2$, $U_b^* = 0$, (c) $U_u^* = 0.2$, $U_l^* = U_b^* = 0$ and (d) $U_u^* = 0.2$, $U_l^* = -0.2$, $U_b^* = 0.2$; $\mathcal{SG}^{\pm}$ denotes surface or external mode, $\mathcal{IG}^{\pm}$ denotes interfacial or internal mode and the $+$ and $-$ signs respectively imply the direction of wave propagation.

is a uniform flow (case 1 of figure 1), there is neither a change in the intrinsic frequency of the waves nor is there a relative Doppler shift between the surface and the interface. However, the bottom ripples are Doppler shifted with respect to the surface and the interface. The dispersion curves for this case has been plotted in figure 2(a) in solid lines. In the dotted lines, we have plotted the dispersion curves without any velocity field. On the vertical axis is the non-dimensionalised frequency ($\omega^* \equiv \omega/\sqrt{g/H}$) and on the horizontal axis is the non-dimensional wavenumber kH. The non-dimensionalised velocity is $U^* \equiv U/\sqrt{gH}$, where $H = h_u + h_l$. All the branches of Doppler shifted dispersion curves are simply U^*kH away from the respective branches without the velocity field.

Figure 2(b) shows the dispersion curve for the case when the shear is in the lower layer only (case 2 of figure 1). Thus the Doppler shift component is the same for both external and internal modes, but the only way this differs from case 1 is by the presence of shear in the lower layer, which has changed the intrinsic frequencies of both external and internal modes.

For the case of shear only in the upper layer (case 3 of figure 1), instead of the pycnocline, the surface undergoes a Doppler shift. Because of shear jump, the intrinsic frequencies of both the branches change. It can be seen from the dispersion curve (figure 2c) that the branches $\mathcal{SG}^+$ and $\mathcal{SG}^-$ are highly non-symmetrical due to
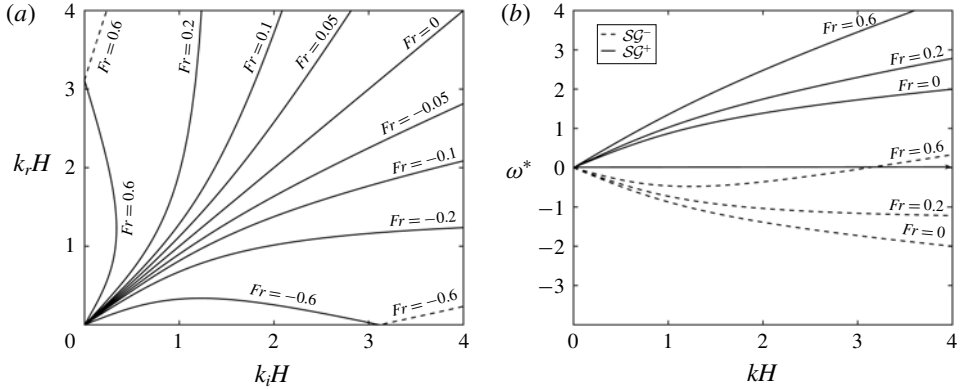
FIGURE 3. (*a*) Different combinations of k_r on $\mathcal{SG}^-$ such that k_i is on $\mathcal{SG}^+$, performed for various values of $Fr \equiv U_u/\sqrt{gH}$ for the case of shear in the lower layer. Here $R = 0.95$ and $h_u/h_l = 1/3$. For solid lines, $k_b = k_i + k_r$ but for dashed lines, $k_b = |k_i - k_r|$. (*b*) Dispersion relations for the same case for three values of *Fr*. Here solid lines represent $\mathcal{SG}^+$ modes and dashed lines represent $\mathcal{SG}^-$.

presence of the velocity U_u at the surface. There is a small change in the intrinsic frequency as well, however, it is not evident from the dispersion curves.

In figure 2(*d*) we have plotted the dispersion curve for the case when both the layers have shear (case 4 of figure 1). For this case, we have assumed the shear to be positive in the upper layer and negative in the lower layer. Thus, the external mode is Doppler shifted positively whereas the internal mode is negatively Doppler shifted.

3.1. *Shear in the lower layer*

Here, we analyse the case when shear is present only in the lower layer and the local velocity at the bottom is zero (case 2 of figure 1). Therefore, the surface modes and the interfacial modes are Doppler shifted by an equal amount with respect to the bottom ripple. Presence of shear will also result in a change in the intrinsic frequencies of the waves. For the case of shear in the lower layer, firstly we investigate the triads formed by two surface modes, i.e. $\mathcal{SG}^+$ and $\mathcal{SG}^-$. We have taken the incident wave k_i on $\mathcal{SG}^+$ and the resonant wave k_r on $\mathcal{SG}^-$. Changing the Froude number changes the resonance condition, as is evident from figure 3(*a*). As mentioned earlier, in the absence of shear, all the Bragg resonance triads having k_i on the $\mathcal{SG}^+$ branch will resonate the waves on the $\mathcal{SG}^-$ branch having $k_r = k_i$. This corresponds to the straight line labelled $Fr = 0.0$ in figure 3(*a*). Increasing Fr ($\equiv U_u/\sqrt{gH}$) will mean that the surface will be positively Doppler shifted with respect to the bottom ripples. For any given positive velocity, at some value of k, the dispersion curve $\mathcal{SG}^-$ is bound to cross the k-axis; see figure 3(*b*). However, while plotting, we have kept the values of k restricted because for higher values of k, even though the resonance condition is satisfied, the rate of energy exchange falls off because the waves are unable to 'feel' the bottom. We see that for $Fr = 0.2$, the $\mathcal{SG}^-$ branch shifts upwards. This is naturally reflected in the change in the resonance condition in figure 3(*b*), in which we have plotted the two branches of the dispersion relation. (The dispersion relation is a fourth-order polynomial in ω but we have plotted only two branches on which the resonance is being studied, i.e. $\mathcal{SG}^+$ and $\mathcal{SG}^-$ in this case.) If *Fr* is

further increased, then for a given k_i on $\mathcal{SG}^+$, there can be up to three values of k_r on $\mathcal{SG}^+$ which would form the triad. This is the reason that for $Fr = 0.6$ curve in figure 3, for a single k_iH, there exist 3 values of k_rH for which resonance condition is met. Two of these triads will be formed if the bottom's wavenumber is $k_b = k_i + k_r$ (shown by the solid line). However, the third k_r would lie on the part of $\mathcal{SG}^-$ for which $\omega > 0$ and for such a triad (shown in broken lines in figure 3a for $Fr = 0.6$), the bottom's wavenumber would be $k_r - k_i$. We note here in passing that these triads represented by the broken lines (in figure 3a, not in 3b) are not 'usual' triads but are 'explosive' triads. In such triads, both the incident wave and the resonant wave grow simultaneously, while the total energy of the system still remains conserved. This is due to the existence of negative energy waves (Cairns 1979). These 'explosive' triads have been explored by McHugh (1992), for capillary–gravity waves, as well as by the authors of this paper (Raj & Guha 2018).

Further, in figure 3(b) we have also plotted the change in the dispersion curves of $\mathcal{SG}^-$ and $\mathcal{SG}^+$ for $Fr = (0, 0.2, 0.6)$ for $kH < 4$. It can be seen that within this window of kH, for a given ω_i on $\mathcal{SG}^+$, there can be only one k_i (lines parallel to the k-axis i.e. $\omega = \pm\omega_0$ intersects any given $\mathcal{SG}^+$ at exactly one point). But for a given $|\omega_r|$ on $\mathcal{SG}^-$, for $Fr = 0.6$, there can be three values of k_r satisfying the dispersion relation, two values are negative and one positive (lines parallel to the k-axis i.e. $\omega = \pm\omega_0$ may intersect any given $\mathcal{SG}^-$ at either one point or at three points).

Although we have discussed the modification in the resonance condition for a positive Fr, a very similar thing happens for a negative Fr. In figure 3, whereas for a positive Fr, there may exist up to three k_r on $\mathcal{SG}^-$ for a given k_i on $\mathcal{SG}^+$, for a negative Fr (see $Fr = 0.6$), three different k_i on $\mathcal{SG}^+$ may resonate the same wavenumber k_r on $\mathcal{SG}^-$ (see, $Fr = -0.6$). Because the dispersion curves in question, i.e. $\mathcal{SG}^+$ and $\mathcal{SG}^-$ are symmetric for $Fr = 0$, the symmetry is also maintained for a positive and a negative Fr.

It might be noticed that the value of Fr needed for any appreciable change in the resonance condition varies from moderate to large. The reason for this is that for surface gravity waves, the intrinsic frequency is quite large and to Doppler shift the intrinsic frequency, a local velocity of similar magnitude is needed. For example, to get three possible resonant waves having $k_rH < 4$ for a given k_iH, a Froude number of approximately 0.5 is needed. However, to Doppler shift the interfacial gravity waves on the pycnocline, a significantly smaller Froude number is sufficient because the intrinsic phase speeds of the interfacial waves are significantly low.

We move on to the incident/resonant wave pairs formed by two interfacial modes, i.e. by the waves on $\mathcal{IG}^+$ and $\mathcal{IG}^-$ for the case of shear in the upper layer (case 3 of figure 1). The pycnocline is not only Doppler shifted with respect to the bottom, but it also has a discontinuity in shear across it. This signifies the presence of vorticity–gravity waves at the pycnocline and a significant change in the intrinsic frequency as well. A figure similar to the previous case showing combinations of k_i (on $\mathcal{IG}^+$) and k_r (on $\mathcal{IG}^-$) has been plotted in figure 4(a) restricting the non-dimensionalised wavenumber to 5. Naturally, at $Fr = 0$, the resonance condition is symmetric but the resonance condition changes greatly even for a small amount of mean flow. As we increase the Fr, for a small k_i on $\mathcal{IG}^+$, the resonance condition is met by a larger k_r on $\mathcal{IG}^-$ (see curves labelled $Fr = 0.01, 0.02$ of figure 4a). On increasing Fr further, again we see the existence of three k_r values for a given k_i, similar to the resonance between $\mathcal{SG}^+$ and $\mathcal{SG}^-$ ($Fr = 0.08$, figure 4a,b). However, if we further keep on increasing Fr, then the complete $\mathcal{IG}^-$ curve will become positive (shown in figure 4b, $Fr = 0.2$) and in such a case, only one resonant wave for any given k_i on $\mathcal{SG}^-$ will
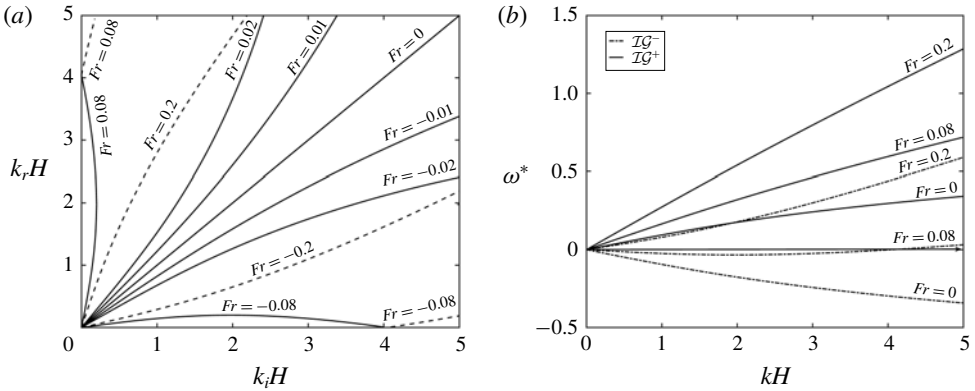
FIGURE 4. (*a*) Different combinations of k_r on $\mathcal{IG}^-$ such that k_i is on $\mathcal{IG}^+$, for various values of Fr when shear is in the lower layer. Here $R = 0.95$ and $h_u/h_l = 1/3$. For solid lines, $k_b = k_i + k_r$ and for dashed lines, $k_b = |k_i - k_r|$. (*b*) Dispersion relations for the same case for three values of Fr. Here solid lines represent $\mathcal{IG}^+$ modes and dashed lines represent $\mathcal{IG}^-$.

exist (dashed line labelled $Fr = 0.2$ in figure 4*a*). The dashed line implies that the wavenumber of the bottom ripple for such a triad is $k_b = k_i - k_r$ unlike the usual case $k_b = k_i + k_r$ for the solid lines in figure 4. Again, similar to the previous case, the triads marked by the dashed lines are the explosive triads. The positive and a negative Fr result in symmetric cases as shown in figure 4.

We put this in the context of a real ocean of depth $H = 100$ m having a pycnocline at $h_u = 25$ m from the surface. These data are similar to those used by Alam *et al.* (2009*b*). In the 'no-flow' situation, an interfacial wave having a wavelength $\lambda_i \sim 200$ m will resonate an oppositely travelling wave of wavelength $\lambda_r \sim 200$ m. However, in the presence of a small velocity of $U_u = U_l = 0.31$ m s^{-1} opposite to the direction of the incident wave, the resonant wave would have a wavelength $\lambda_r \sim 140$ m.

The third sub-case for the case of shear in the upper layer is the resonant interaction between a surface and interfacial mode having opposite intrinsic frequency. This means that the incident/resonant pair is either $\mathcal{IG}^+/\mathcal{SG}^-$ or $\mathcal{IG}^-/\mathcal{SG}^+$. Without a loss of generality, we will discuss only the $\mathcal{IG}^+/\mathcal{SG}^-$ pair; see figure 5(*a,b*). The results about the other pair can be obtained in a straightforward manner, simply by changing the sign of Fr from positive to negative and *vice versa*. What matters is that whether the sign of mean flow and that of surface/interfacial waves are in the same direction or the opposite. The positive shear in this particular case will imply that the velocity at the surface/pycnocline is in the direction of the propagation of the interfacial wave $\mathcal{IG}^+$. Therefore, increasing Fr will lead to an increase in the frequency of $\mathcal{IG}^+$ but a non-monotonic change in the frequency of the $\mathcal{SG}^-$ mode, as shown in figure 5(*b*). Even for a small value of shear, the effect on the speed of $\mathcal{IG}^+$ is significant but $\mathcal{SG}^-$ is relatively less affected. However, for a large value of Fr, there may exist multiple values of k_r for a given k_i as can be seen from figure 5(*a*), $Fr = 0.3$, 0.4, 0.5, 0.6. The reason is simply a non-monotonic behaviour of frequency of $\mathcal{SG}^-$ with respect to the wavenumber as can be seen from figure 5(*b*). For a higher value of Fr, the frequency of $\mathcal{SG}^-$ becomes positive and the triads formed by the positive part of $\mathcal{SG}^-$ are shown in dashed lines in figure 5(*a*). For these triads (again these triads are explosive), the bottom's wavenumber is $k_r - k_i$ whereas for triads marked by solid line, the bottom's wavenumber is $k_r + k_i$.
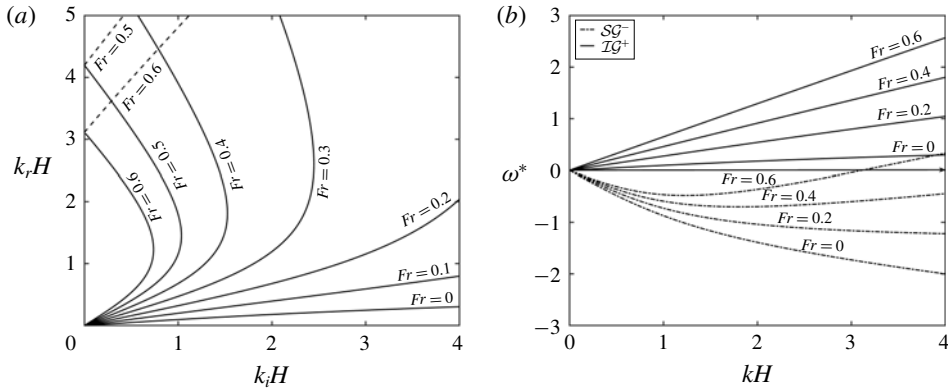
FIGURE 5. (*a*) Different combinations of k_r on $\mathcal{SG}^-$ such that k_i is on $\mathcal{IG}^+$, for various positive *Fr* values when shear is in the lower layer. Here $R = 0.95$ and $h_u/h_l = 1/3$. For solid lines, $k_b = k_i + k_r$ but for dashed lines, $k_b = |k_i - k_r|$. (*b*) Dispersion relations for the same case for different increasingly positive *Fr*. Here solid lines represent $\mathcal{IG}^+$ modes and dashed lines represent $\mathcal{SG}^-$.
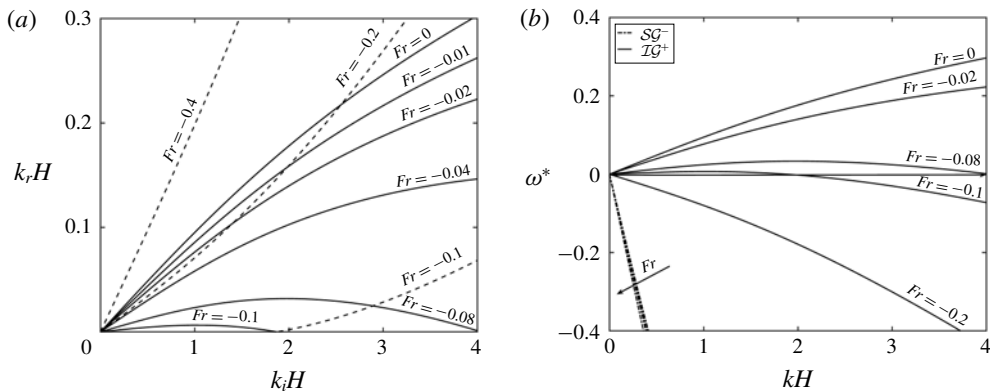

FIGURE 6. (*a*) Different combinations of k_r on $\mathcal{SG}^-$ such that k_i is on $\mathcal{IG}^+$, for various negative *Fr* values when shear is in the lower layer. Here $R = 0.95$ and $h_u/h_l = 1/3$. For solid lines, $k_b = k_i + k_r$ but for dashed lines, $k_b = |k_i - k_r|$. (*b*) Dispersion relations for the same case for different negative *Fr*. Direction of arrows imply increasingly negative *Fr*. Here solid lines represent $\mathcal{IG}^+$ modes and dashed lines represent $\mathcal{SG}^-$.

If the Froude number is negative (see figure 6*a*,*b*), the frequency of $\mathcal{SG}^-$ increases monotonically but that of $\mathcal{IG}^+$ may become non-monotonic; shown in figure 6(*b*) for the case $Fr = -0.08$. Because the frequency of $\mathcal{SG}^-$ plotted in figure 6(*b*) is restricted, not much difference in the dispersion curves is obtained. For a higher *Fr*, the frequency changes sign within the chosen limit of $kH = 4$ and becomes negative ($Fr = -0.1$). For a further increase in the velocity, the frequency becomes completely negative for $\mathcal{IG}^-$ ($Fr = -0.2$). This change in the frequency is reflected in the change in the resonance condition and the change can be visualised in figure 6(*a*). For $Fr = -0.01, -0.02, -0.04$, for a single k_r, only one $k_i < 4$ exists but for higher *Fr*, a single k_r maybe resonant by multiple k_i ($Fr = -0.08, -0.1$). For $Fr = -0.1$, the bottom's
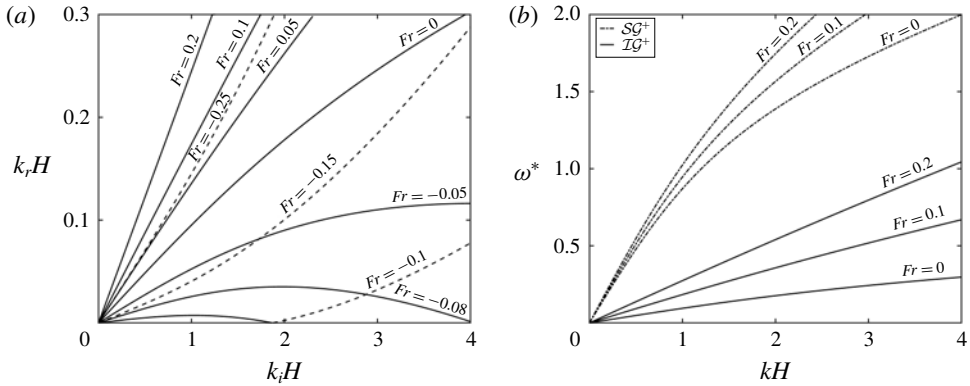
FIGURE 7. (a) Different combinations of k_r on $\mathcal{SG}^+$ such that k_i is on $\mathcal{IG}^+$ for various values of positive Fr and for low values of negative Fr for the case of shear in the lower layer; $R = 0.95$, $h_u/h_l = 1/3$. For solid lines, $k_b = |k_i - k_r|$ and for dashed lines, $k_b = k_i + k_r$. (b) Dispersion relation for positive Fr. Here solid lines represent $\mathcal{IG}^+$ modes and dashed lines represent $\mathcal{SG}^+$.

wavenumber is $k_i + k_r$ for the solid line part in figure 6(a) and $k_i - k_r$ for the dashed line part i.e. the explosive triads.

Finally, we deal with the case when the incident/resonant modes are in the same direction i.e. $\mathcal{IG}^+/\mathcal{SG}^+$ or $\mathcal{IG}^-/\mathcal{SG}^-$. Again, without a loss of generality, we study only the resonance between $\mathcal{IG}^+/\mathcal{SG}^+$ modes and in this case, positive Fr will imply a flow in the same direction of the waves; see figure 7(a,b). Because all the involved waves and the mean flow are in the same direction, there is no question of sign changing of the frequency of any wave. The frequencies of all the waves increases progressively with increasing Fr (figure 7b). In figure 7(a,b), however, we have plotted both the positive Fr and the negative Fr having low magnitudes. Increasing Fr will mean that for a given k_i, a higher k_r will be needed for resonance which can be seen from figure 7(a,b) (positive Fr).

For a negative Fr (see figure 8a,b), the dispersion relation is plotted in figure 8(b). For $Fr = -0.1$, $\mathcal{SG}^+$ is positive throughout but a part of $\mathcal{IG}^+$ becomes negative. For a higher negative Fr (say -0.3), $\mathcal{SG}^+$ remains positive, but $\mathcal{IG}^+$ becomes completely negative. For a further negative Fr, $\mathcal{IG}^+$, remains negative and a part of $\mathcal{SG}^+$ also becomes negative. The effect on the resonance conditions for the case of small negative Fr (up to -0.25) has been plotted in figure 7(a) and for higher negative Fr has been plotted in figure 8(a).

3.2. *Shear in the upper layer*

As we have mentioned earlier, shear in the upper layer causes a relative Doppler shift between the surface and the pycnocline, as well as the bottom ripple. Further, the change in the intrinsic frequencies of the surface modes will be minimal compared to the change in the intrinsic frequencies of the interfacial modes. In §3.1, we have performed a detailed study on how the Doppler shift changes the resonance conditions. Here we focus on the case when the intrinsic frequency of the waves changes, and because the intrinsic frequencies of the interfacial waves are more prone to change, the case of substantial interest is the resonant interaction between the $\mathcal{IG}^+$ and $\mathcal{IG}^-$ modes. Since shear is only in the upper layer and the pycnocline has no local base
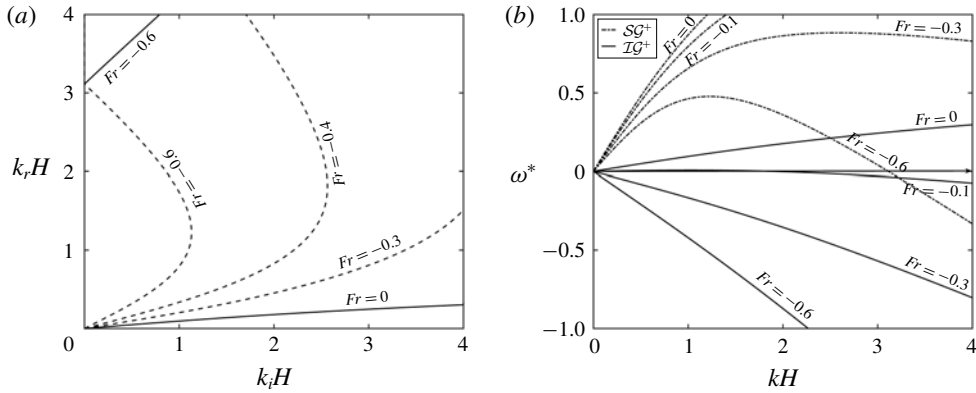
FIGURE 8. (*a*) Different combinations of k_r on $\mathcal{SG}^+$ such that k_i is on $\mathcal{IG}^+$ for high values of negative Fr for the case of shear in the lower layer. Here $R = 0.95$ and $h_u/h_l = 1/3$. For solid lines, $k_b = |k_i - k_r|$ and for dashed lines, $k_b = k_i + k_r$. (*b*) Dispersion relation for negative Fr. Here solid lines represent $\mathcal{IG}^+$ modes and dashed lines represent $\mathcal{SG}^+$.
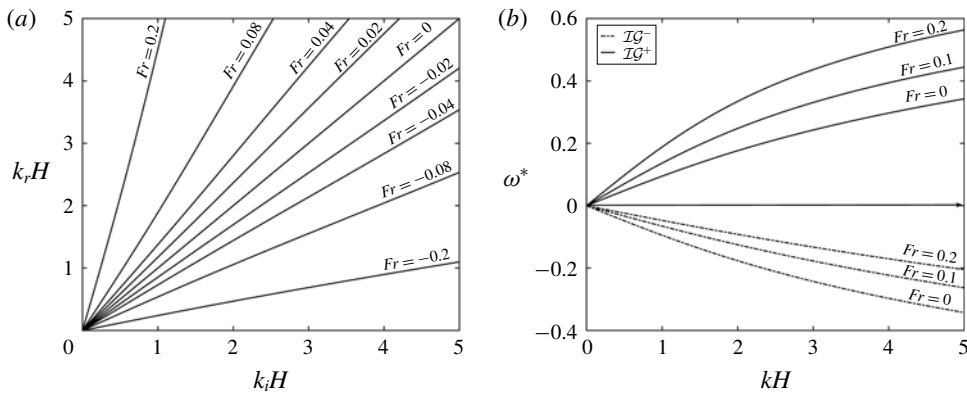

FIGURE 9. (*a*) Different combinations of k_r on $\mathcal{IG}^-$ such that k_i is on $\mathcal{IG}^+$, for various values of $Fr \equiv U_u/\sqrt{gH}$ when shear is in the upper layer. Here $U_l = U_b = 0$, $R = 0.95$ and $h_u/h_l = 1/3$. (*b*) Dispersion relations for the same case for three values of Fr.

velocity, there is no role of the Doppler shift. However, when shear in the upper layer is positive ($Fr > 0$), $\mathcal{IG}^+$ is sped up but the $\mathcal{IG}^-$ mode is slowed down (we note that the wave at the interface is a vorticity–gravity wave). Although for the $Fr = 0$ case, the resonant wave is $k_r = k_i$, the conditions change when $Fr \neq 0$. For $Fr > 0$, we have $k_r < k_i$, and for $Fr < 0$, we get $k_r > k_i$. The change in the resonance condition is shown in figure 9(*a*) and the dispersion relation for $Fr > 0$ has been plotted in figure 9(*b*).

4. Wave triad in the presence of a base velocity field

4.1. *Uniform flow and consequences of shear*

Wave triad interaction is an energy exchange between waves on the surface and the pycnocline and there is no direct involvement of bottom topography. Therefore, a velocity field with a uniform flow (figure 1 case 1) will Doppler shift the waves on the surface and the pycnocline by the same velocity U and there will not be

any consequences for the resonance condition. To illustrate this, we take three waves having wavenumbers (k_1, k_2, k_3) and corresponding frequencies $(\omega_1, \omega_2, \omega_3)$ such that $k_1 + k_2 - k_3 = 0$ but $\omega_1 + \omega_2 - \omega_3 \neq 0$. In the presence of a constant base velocity U, every frequency ω_j $(j = 1, 2, 3)$ would be Doppler shifted by an amount Uk_j. In such a case, however, the intrinsic frequencies of the waves will undergo no change. Therefore, the modified frequency condition would be

$$
\begin{aligned}
(\omega_1 + Uk_1) &+ (\omega_2 + Uk_2) - (\omega_3 + Uk_3) \\
&= \omega_1 + \omega_2 - \omega_3 + U(k_1 + k_2 - k_3) \\
&= \omega_1 + \omega_2 - \omega_3 \\
&\neq 0.
\end{aligned}
\tag{4.1}
$$

Thus, a mere Doppler shift by the same velocity U would not change the resonance condition for the wave triad interaction. However, if the surface and the interface were to be Doppler shifted by different amounts, there can be changes in the resonance conditions and naturally the three waves satisfying the resonance condition in the absence of shear might not do so in the presence of a shear. Alternatively, three waves not satisfying a resonance condition might do so in the presence of velocity shear. This can be elucidated using a simple example: let $k_1 + k_2 - k_3 = 0$ but $\omega_1 + \omega_2 - \omega_3 \neq 0$, i.e. the waves do not satisfy the resonant condition in the absence of a base velocity shear. Let us assume that the waves 1 and 2 are at the surface, which now has a base velocity U_u, while wave 3 is at the interface, which travels with a velocity U_l (different from U_u because of shear). Then, the frequency condition reads

$$
\begin{aligned}
(\omega_1' + U_u k_1) &+ (\omega_2' + U_u k_2) - (\omega_3' + U_l k_3) \\
&= \omega_1' + \omega_2' - \omega_3' + U_u(k_1 + k_2) - U_l k_3 \\
&= 0 \quad \text{iff} \quad \omega_1' + \omega_2' - \omega_3' = k_3(U_l - U_u).
\end{aligned}
\tag{4.2}
$$

The primes in the frequencies denote that the intrinsic frequencies will be modified due to shear.

4.2. *Shear in the lower layer*

When shear is present only in the lower layer, there is no Doppler shift between the two waves and the only effect of the shear is felt in modifying the intrinsic frequencies of the waves. Although the shear jump is only at the pycnocline, the effect of it at lower wavenumbers would be felt in the surface mode as well. In figure 10(a), we have shown the change in the resonance condition for three interacting waves having k_1, k_2 and k_3 on $\mathcal{IG}^-$, $\mathcal{SG}^-$ and $\mathcal{IG}^+$ respectively. The Froude numbers are as follows: $Fr = (0.0, 0.2, 0.4, 0.6)$. As the shear is increased in the positive direction, for a given k_1 on $\mathcal{IG}^-$, k_2 on $\mathcal{SG}^-$ decreases but k_3 on $\mathcal{IG}^+$ increases. The figure reveals that the change is not as significant as that in the Bragg resonance case even at high values of shear.

4.3. *Shear in the upper layer*

The presence of a shear in the upper layer modifies the flow in two ways. Firstly, there now exists a jump in base shear both at the surface and at the interface, which changes the intrinsic frequencies of all four modes. Secondly, the presence of shear automatically means that the local mean velocities at the surface and at
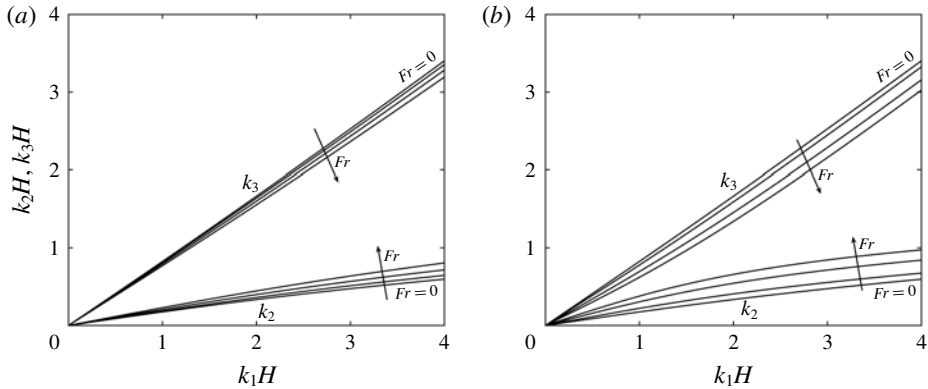
FIGURE 10. Different combinations of k_1, k_2 and k_3 on $\mathcal{IG}^-$, $\mathcal{SG}^-$, $\mathcal{IG}^+$ respectively forming a resonance triad for (*a*) shear in bottom layer only; $U_u^* = U_l^* = (0.0, 0.2, 0.4, 0.6)$, $U_b^* = 0$, $R = 0.95$ and $h_u/h_l = 1/3$. (*b*) Shear in top layer only; $U_u^* = (0.0, 0.2, 0.4, 0.6)$, $U_l^* = U_b^* = 0$, $R = 0.95$ and $h_u/h_l = 1/3$.

the pycnocline are different from each other, which implies a relative Doppler shift between the two. Although such a situation may give rise to shear instabilities, such shear instabilities tend to occur at higher wavenumbers which have very low growth rates. In figure 10(*b*), we have shown the resonance condition for three interacting waves having k_1, k_2 and k_3 respectively on $\mathcal{IG}^-$, $\mathcal{SG}^-$ and $\mathcal{IG}^+$. Yet again, the behaviour is similar to that of the previous case but the change in the resonance condition is more prominent here due to the Doppler shifting of the surface and the interface.

5. Numerical method

Higher-order spectral (HOS) method is a highly accurate and efficient numerical method developed by Dommermuth & Yue (1987) for studying wave propagation and wave–topography interaction for a single-layered fluid. Among other things, they studied the collision of two wave packets. The method was further expanded to a two-layered density stratified fluid by Alam *et al.* (2009*b*) to study various cases of Bragg resonance. Although in § 2 we have derived the evolution equations analytically assuming the resonance conditions are exactly satisfied, the HOS code allows us to simulate the near-resonance conditions as well. Furthermore, the study of multiple resonances, which would be a tedious analytical exercise, becomes simpler on using the HOS method. Here our objective is to extend the versatile HOS method to incorporate a piecewise linear velocity field. The base velocity field thus introduced will be continuous but its z-derivative might be discontinuous at the interfaces, thus giving rise to vorticity–gravity waves. In our formulation, we specify the values of the base velocities at $h = \{0, -h_u, -h_u - h_l\}$ as $U = \{U_u, U_l, U_b\}$, using which we get various sub-cases. For $U_u = U_l = U_b = 0$, our system will reduce to the system studied in Alam *et al.* (2009*b*), i.e. having four pure gravity waves with no shear. Furthermore, setting $U_u = U_l = U_b \neq 0$ would lead to gravity waves whose frequencies are simply Doppler shifted with respect to the bottom.

In the HOS method, we solve the evolution of the surface and interface elevations and velocity potentials associated with them. The rest of the variables in the fluid

bulk are solved analytically using the boundary conditions. Since the major part of the computation is limited to the surface and the interface, the HOS method is highly computationally efficient. We proceed similar to what has been described in Alam *et al.* (2009*b*), using similar notations. The continuity equations read

$$\nabla^2 \phi_u = 0 \quad -h_u + \eta_l < z < \eta_u, \tag{5.1a}$$

$$\nabla^2 \phi_l = 0 \quad -h_u - h_l + \eta_b < z < -h_u + \eta_l. \tag{5.1b}$$

The kinematic boundary conditions are as follows:

$$\eta_{u,t} + (U + \phi_{u,x})\eta_{u,x} = \phi_{u,z} \quad \text{at } z = \eta_u, \tag{5.2a}$$

$$\eta_{l,t} + (U + \phi_{u,x})\eta_{l,x} = \phi_{u,z} \quad \text{at } z = -h_u + \eta_l, \tag{5.2b}$$

$$\eta_{l,t} + (U + \phi_{l,x})\eta_{l,x} = \phi_{l,z} \quad \text{at } z = -h_u + \eta_l, \tag{5.2c}$$

$$(U + \phi_{l,x})\eta_{b,x} = \phi_{l,z} \quad \text{at } z = -h_u - h_l + \eta_b. \tag{5.2d}$$

Likewise, for the dynamic boundary conditions, we have

$$\phi_{u,t} + \tfrac{1}{2}(\phi_{u,x}^2 + \phi_{u,z}^2) + U\phi_{u,x} - \Omega_u \psi_u + g\eta_u = 0 \quad \text{at } z = \eta_u, \tag{5.3a}$$

$$\rho_u \left[\phi_{u,t} + \tfrac{1}{2}(\phi_{u,x}^2 + \phi_{u,z}^2) + U\phi_{u,x} - \Omega_u \psi_u + g\eta_l \right]$$
$$- \rho_l \left[\phi_{l,t} + \tfrac{1}{2}(\phi_{l,x}^2 + \phi_{l,z}^2) + U\phi_{l,x} - \Omega_l \psi_l + g\eta_l \right] = 0 \quad \text{at } z = -h_u + \eta_l. \tag{5.3b}$$

The governing equations for the potential are simply the Laplace equations, which cannot accommodate time evolution, by itself. However, there is a time evolution equation for the potentials at the surface and the interface, which are given by the dynamic boundary conditions. We define a surface potential and an interface potential, whose evolution can be tracked using the two dynamic boundary conditions:

$$\phi^S(x, t) \equiv \phi_u(x, \eta_u(x, t), t), \tag{5.4a}$$

$$\phi_u^I(x, t) \equiv \phi_u(x, -h_u + \eta_l(x, t), t), \tag{5.4b}$$

$$\phi_l^I(x, t) \equiv \phi_l(x, -h_u + \eta_l(x, t), t). \tag{5.4c}$$

Further, we define a new potential at the interface using the above defined potentials:

$$\phi^I(x, t) \equiv \phi_l^I(x, t) - R\phi_u^I(x, t). \tag{5.5}$$

Additionally, we define surface and interface streamfunctions

$$\psi^S(x, t) \equiv \psi_u(x, \eta_u(x, t), t), \tag{5.6a}$$

$$\psi_u^I(x, t) \equiv \psi_u(x, -h_u + \eta_l(x, t), t), \tag{5.6b}$$

$$\psi_l^I(x, t) \equiv \psi_l(x, -h_u + \eta_l(x, t), t). \tag{5.6c}$$

Using the kinematic and dynamic boundary conditions, we obtain the evolution equations for the surface potential, ϕ^S, the interface potential, ϕ^I, the surface elevation, η_u, and the interface elevation, η_l:

$$\eta_{u,t} = -\eta_{u,x}[\phi_{u,x}^S + U_u + \Omega_u \eta_u] + (1 + \eta_{u,x}^2)\phi_{u,z} \quad \text{at } z = \eta_u, \tag{5.7a}$$

$$\eta_{l,t} = -\eta_{l,x}[\phi_{l,x}^I + U_l + \Omega_l \eta_l] + (1 + \eta_{l,x}^2)\phi_{l,z} \quad \text{at } z = -h_u + \eta_l, \tag{5.7b}$$

$$\phi_{,t}^S = -g\eta_u - \tfrac{1}{2}(\phi_{u,x}^S)^2 + \tfrac{1}{2}(1+\eta_{u,x}^2)\phi_{u,z}^2 - (U_u + \Omega_u\eta_u)\phi_{u,x}^S + \Omega_u\psi^S \quad \text{at } z = \eta_u, \quad (5.7c)$$

$$\begin{aligned}
\phi_{,t}^I = {} & \tfrac{1}{2}(R(\phi_{u,x}^I)^2 - (\phi_{l,x}^I)^2) + \tfrac{1}{2}(1+\eta_{l,x}^2)(\phi_{l,z}^2 - R\phi_{u,z}^2) - g\eta_l(1-R) + U_l(R\phi_{u,x}^I - \phi_{l,x}^I) \\
& - R\Omega_u\psi_u^I + \Omega_l\psi_l^I + \eta_l(R\Omega_u\phi_{u,x}^I - \Omega_l\phi_{l,x}^I) \quad \text{at } z = -h_u + \eta_l.
\end{aligned} \quad (5.7d)$$

In the above equations, we have substituted the Taylor expansion for U (see (2.6) and (2.7)). The velocity potential and the streamfunctions are expanded in a perturbation series:

$$\phi_{u/l}(x, z, t) = \sum_{m=1}^{M} \phi_{u/l}^{(m)}(x, z, t); \quad \psi_{u/l}(x, z, t) = \sum_{m=1}^{M} \psi_{u/l}^{(m)}(x, z, t). \quad (5.8a,b)$$

At every order m, we further write the velocity potentials as a sum of basis functions (Fourier basis function in this case). Assuming solutions to be periodic in the x-direction, we express the solutions as a discrete Fourier series. (It is necessary to filter out the high wavenumbers by applying a low pass filter, so that the amplification of round off errors at higher wavenumbers does not happen; see § 3.2.2 of Dommermuth & Yue (1987).) Furthermore, we use the Laplace equations to find the function form of the solutions, and we finally get

$$\phi_u^{(m)} = \sum_{n=-N}^{N-1} \left[A_n^{(m)}(t)\frac{\cosh k_n(z + h_u)}{\cosh(k_n h_u)} + B_n^{(m)}(t)\frac{\sinh(k_n z)}{\cosh(k_n h_u)} \right] e^{ik_n x}, \quad (5.9)$$

$$\phi_l^{(m)} = \sum_{n=-N}^{N-1} \left[C_n^{(m)}(t)\frac{\cosh k_n(z + h_u + h_l)}{\cosh(k_n h_l)} + D_n^{(m)}(t)\frac{\sinh k_n(z + h_u + h_l)}{\cosh(k_n h_l)} \right] e^{ik_n x}. \quad (5.10)$$

However, it would not be convenient to directly substitute (5.9) and (5.10) in the boundary conditions to obtain the unknown coefficients because at the surface and the interface, z will have a dependence on x. Hence, we expand the surface and interface potentials as a Taylor series about the respective mean level, so as to eliminate the implicit x-dependence of the eigenfunctions:

$$\phi^S(x, t) = \sum_{m=1}^{M} \phi_u^{(m)}(x, \eta_u, t) = \sum_{m=1}^{M}\sum_{k=0}^{M-m} \frac{\eta_u^k}{k!}\frac{\partial^k}{\partial z^k}\phi_u^{(m)}(x, z, t)\bigg|_{z=0}. \quad (5.11)$$

The above equation can be written as a sequence of Dirichlet boundary conditions at each order m. Here, the boundary conditions at each order depend on the product of the terms which have already been found out at the leading orders, therefore making the problem effectively linear at every order m. Further details on the derivation of the boundary conditions can be found in appendix B. We have

$$\phi_u^{(m)}(x, 0, t) = f_u^{(m)}, \quad (5.12)$$

where

$$f_u^{(1)} = \phi^S, \quad (5.13)$$

$$f_u^{(m)} = -\sum_{k=1}^{m-1} \frac{\eta_u^k}{k!}\frac{\partial^k}{\partial z^k}\phi_u^{(m-k)}(x, z, t)\bigg|_{z=0}. \quad (5.14)$$

Similarly, for the interface we have a similar sequence of Dirichlet boundary conditions:

$$\Phi^{(m)}(x, -h_u, t) = f_{l1}^{(m)},\tag{5.15}$$

where

$$f_{l1}^{(1)} = \phi^I,\tag{5.16}$$

$$f_{l1}^{(m)} = -\sum_{k=1}^{m-1}\frac{\eta_l^k}{k!}\frac{\partial^k}{\partial z^k}\Phi^{(m-k)}(x, z, t)\Bigg|_{z=-h_u}.\tag{5.17}$$

Here we have defined $\Phi(x, z, t) \equiv \phi_l(x, z, t) - R\phi_u(x, z, t)$. As for the third boundary condition, we write

$$\varphi_{,z}(x, z, t) = \eta_{l,x}\varphi_{,x}(x, z, t) + \eta_l\eta_{l,x}(\Omega_u - \Omega_l)\quad\text{at } z = -h_u + \eta_l,\tag{5.18}$$

with $\varphi(x, z, t) \equiv \phi_u(x, z, t) - \phi_l(x, z, t)$. Using the Taylor expansion of $\varphi(x, z, t)$ about the mean interface level along with the Laplace equation, we finally get a sequence of Neumann boundary conditions:

$$\varphi_{,z}^{(m)}(x, -h_l, t) = f_{l2}^{(m)},\tag{5.19}$$

where

$$f_{l2}^{(1)} = 0,\tag{5.20}$$

$$f_{l2}^{(2)} = \frac{\partial}{\partial x}[\eta_l\varphi_{,x}^{(1)}(x, z, t)|_{z=-h_u}] + \eta_l\eta_{l,x}(\Omega_u - \Omega_l)\tag{5.21}$$

$$f_{l2}^{(m)} = \sum_{k=1}^{m-1}\frac{\partial}{\partial x}\left[\frac{\eta_l^k}{k!}\frac{\partial^{k-1}}{\partial z^{k-1}}\varphi_{,x}^{(m-k)}(x, z, t)\Bigg|_{z=-h_u}\right].\tag{5.22}$$

Finally, for the bottom boundary condition, we have a similar impenetrability boundary condition:

$$\phi_{l,z}^{(m)}(x, -h_u - h_l, t) = f_b^{(m)},\tag{5.23}$$

where

$$f_b^{(1)} = U_b\eta_{b,x},\tag{5.24}$$

$$f_b^{(2)} = \frac{\partial}{\partial x}[\eta_b\phi_{l,x}^{(1)}(x, z, t)|_{z=-h_u-h_l}] + \eta_b\eta_{b,x}\Omega_l\tag{5.25}$$

$$f_b^{(m)} = \sum_{k=1}^{m-1}\frac{\partial}{\partial x}\left[\frac{\eta_b^k}{k!}\frac{\partial^{k-1}}{\partial z^{k-1}}\phi_{l,x}^{(m-k)}(x, z, t)\Bigg|_{z=-h_u-h_l}\right].\tag{5.26}$$

Using the four boundary conditions, we obtain the value of unknown coefficients A_n, B_n, C_n and D_n at every order m. Now we have a full solution of $\phi_u^{(m)}$ and $\phi_l^{(m)}$ at the order m. At the next order $m + 1$, the functions f_u, f_{l1}, f_{l2}, f_b can be evaluated by using the velocity potentials and their derivatives, which were already found out at the previous order m. Again the boundary value problem at the order $m + 1$ can be solved, and in this way we can proceed further to obtain $\phi_u^{(m)}$ and $\phi_l^{(m)}$ at each order. It is interesting to note here that the all the above four boundary conditions – (5.12), (5.15), (5.19), (5.23) are the same as those in Alam *et al.* (2009*b*), i.e. without
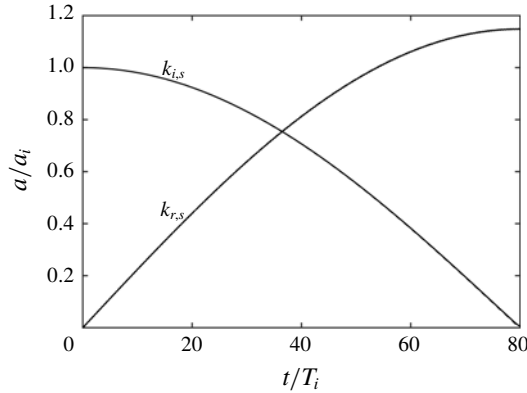
FIGURE 11. Code validation for $R = 0.98$, $k_i H = 0.086$, $k_r H = 0.1140$, $k_b H = 0.2$, $\omega_i^* = 0.0982$, $\omega_r^* = -0.0982$, $U_u^* = 0.1864$, $U_l^* = 0.0083$, $M = 3$, $N = 2048$, $T_i/\Delta T = 512$. The analytical and numerical solutions are indistinguishable.

a background velocity. Therefore, the function form of the coefficients A_n, B_n, C_n and D_n in terms of the functions f_u, f_{l1}, f_{l2} and f_b remain the same. Using these coefficients, we can find any derivative of the velocity potentials at any location. After solving the boundary value problem, we march forward in time using a fourth-order Runge–Kutta method. The domain size is chosen to be 2π and the number of points in real space equals $2N + 1$ such that variables are periodic in x.

5.1. *Validation*

A comprehensive benchmarking of the HOS method for two layers without a velocity field has been performed in Alam *et al.* (2009*b*). In this paper, we have extended the method to incorporate the velocity field by adding requisite terms. For validation of the code, we have simulated a case of Bragg resonance in which the surface mode interacts with the bottom to generate another surface mode having an intrinsic frequency of the opposite sign. We have compared the solution of the HOS code to the analytically obtained solution. The parameters used are mentioned in the caption of figure 11. It can be seen that the analytical solution and the numerical solution are graphically indistinguishable.

5.2. *Numerical results*

We have simulated a resonance between the waves on the same branch ($\mathcal{SG}^-$) of the dispersion curve for case 2, i.e. shear only in the lower layer. The incident wave has the wavenumber $k_i H = 0.83$, while the resonant wave has the wavenumber $k_r H = 2.27$. These two waves have the same direction of propagation and have the same frequency of $\omega^* = -0.4770$. Because the direction of propagation of the waves is the same, the wavenumber of the bottom is the difference of the wavenumber of the incident and the resonant waves, i.e. $k_b H = 1.44$. The velocities are $U_u^* = 0.5016$, $U_l^* = 0$, $U_b^* = 0$. Other relevant physical parameters are $h_u/h_l = 1/3$ and $R = 0.95$. The dispersion relation is plotted in figure 12(*a*) and the corresponding HOS simulation is shown in figure 12(*b*).

Next, we have studied the effect of shear in the upper layer on the Bragg resonance between two oppositely travelling internal modes, i.e. $\mathcal{IG}^+$ and $\mathcal{IG}^-$. Because the

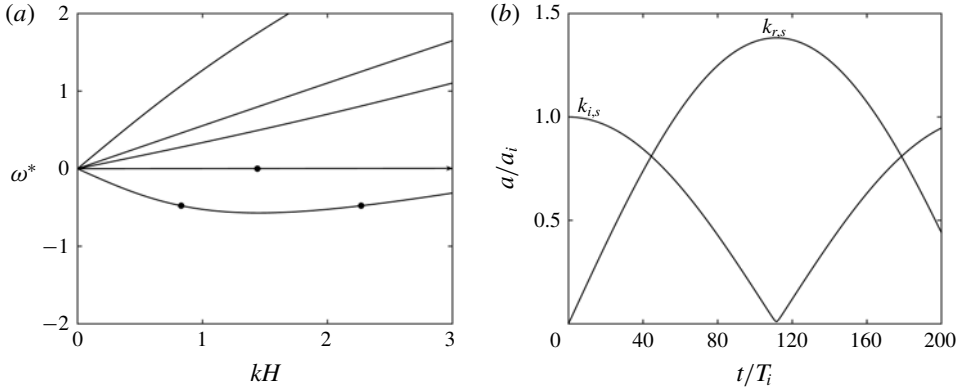FIGURE 12. (*a*) Dispersion relation showing the location of the resonant triad. Both the incident and the resonant waves lie on the $\mathcal{SG}^-$ curve. (*b*) Numerical simulation using the HOS code: $a_i = 0.00005H$, $a_b = 0.02H$, $U_u^* = 0.5016$, $U_l^* = U_b^* = 0$, $\omega_i^* = -0.4770$, $R = 0.95$, $k_i H = 0.83$, $k_r H = 2.27$, $k_b H = 1.44$, $h_u/h_l = 1/3$, $M = 3$, $N = 1024$, $T_i/\Delta T = 2048$. T_i is the time period of the incident wave.

shear is in the upper layer only, there is no Doppler shift of the concerned waves (both on the pycnocline), and the changes are only in the intrinsic frequencies. In the absence of a base flow, it is known that the resonant wavenumber will be the same as the incident wavenumber. However, we have shown analytically in § 4.1 that shear changes the resonance condition. To illustrate this here, we take our incident wave on $\mathcal{IG}^+$ having wavenumber $k_i H = 0.10$ and frequency $\omega_i^* = 0.0097$. The bottom ripple consists of three different wavenumbers: $k_{b1} H = 0.19$, $k_{b2} H = 0.20$ and $k_{b3} H = 0.21$. Thus, the incident wave will interact with the bottom and may generate three different waves having wavenumbers $k_{r1} H = 0.09$, $k_{r2} H = 0.10$, $k_{r3} H = 0.11$ and frequencies $\omega_{r1}^* = -0.0088$, $\omega_{r2}^* = 0.0097$, $\omega_{r3}^* = -0.0107$ respectively. Only one of these wavenumbers may satisfy a resonance condition for a given velocity field and the other wavenumbers will be generated in a 'near-resonant' way (Craik 1988). We plot the time evolution of amplitude of all these three wavenumbers in the absence of shear; see figure 13(*a*). As expected, the maximum growth is only in the wavenumber $k_{r2} H = 0.10$. The amplitude plotted is simply the spatial Fourier transform of the interface, and a rapidly changing amplitude corresponding to $kH = 0.10$ signifies an oppositely travelling wave increasing in amplitude. At approximately $t/T_0 \approx 30$, both the positively and the negatively travelling waves have the same amplitude. We also observe a small growth in the wavenumbers $kH = 0.09$ and $kH = 0.11$. These two wavenumbers do not satisfy the exact resonant condition and hence are generated only near resonantly.

Next, we make the shear negative in the upper layer to yield $U_u^* = -0.0136$, while keeping $U_l^* = U_b^* = 0$. Due to the velocity field, the incident wave's frequency gets modified to $\omega_i^* = 0.0092$. The frequencies of the three possible resonant waves respectively become $\omega_{r1}^* = -0.0092$, $\omega_{r2}^* = -0.0103$ and $\omega_{r3}^* = -0.0103$. In this case, we observe that the incident wave frequency is equal to ω_{r1}, therefore the dominant resonating wavenumber is $k_{r1} H = 0.09$. The amplitude evolution has been plotted in figure 13(*b*). Wiggles in the plot indicate near-resonant generation of oppositely travelling waves.

Likewise, we make the shear positive in the upper layer to yield $U_u^* = 0.0123$, while keeping $U_l^* = U_b^* = 0$. The incident wave's frequency changes to $\omega_i^* = 0.0102$.
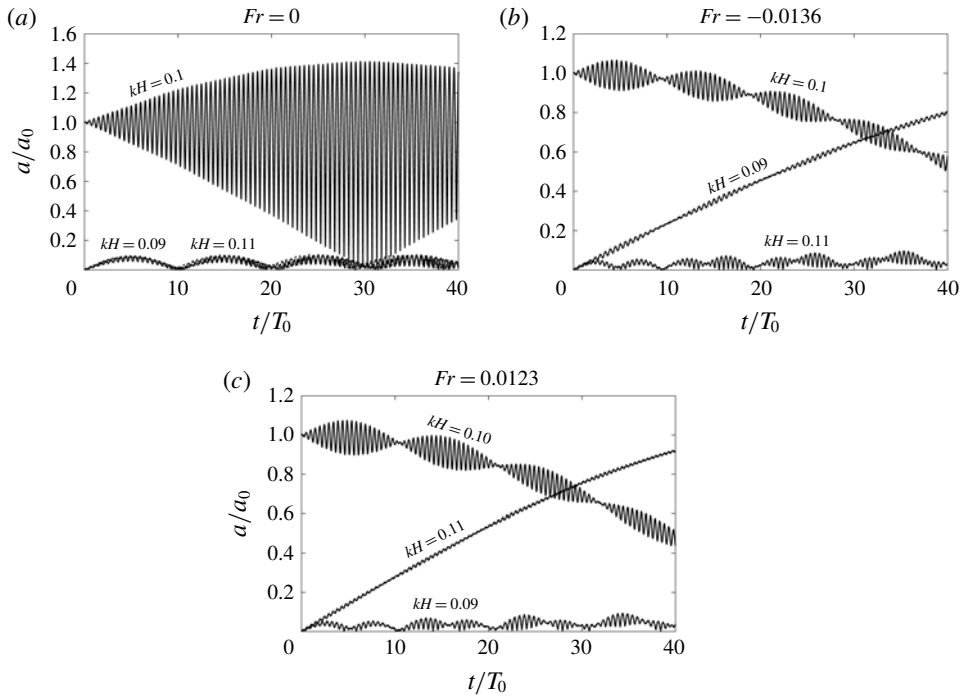
FIGURE 13. Amplitude versus time plot for different wavenumbers on the interface for $R = 0.95$, $h_u/h_l = 1/3$, $a_i = 0.00005H_0$, $a_b = 0.05H_0$ and $U_l^* = U_b^* = 0$. (a) $U_u^* = 0$, (b) $U_u^* = -0.0136$ and (c) $U_u^* = 0.0123$. Parameters for the simulation are $M = 3$, $N = 512$, $T_0/\Delta T = 512$. Here, T_0 is the time period of the wave k_i in the absence of any background velocity.

The frequency of the three possible resonant waves become $\omega_{r1}^* = -0.0083$, $\omega_{r2}^* = -0.0093$ and $\omega_{r3}^* = -0.0102$. We observe that $\omega_i = \omega_{r3}$ and hence, the dominant wavenumber generated is $k_{r3}H = 0.11$. This also corroborates figure 9, where it can be seen that for a k_i on the $\mathcal{IG}^+$ mode, increasing the shear results in an increase in k_r on the $\mathcal{IG}^-$ mode. The amplitude evolution has been plotted in figure 13(c). Again, wiggles indicate near-resonant generation of oppositely travelling waves. Thus, we see that the exclusion of shear may substantially change the condition for resonant triads. Hence, practical applications, such as broadband cloaking (Alam 2012), in which bottom corrugations are designed in a particular way to 'cloak' the offshore structures, may need to account for oceanic shear for an optimum design.

6. Summary and conclusion

Four wave modes, two at the surface and two at the pycnocline, exist in two-layered density stratified flows. A set of three modes can form a triad and undergo weakly nonlinear interactions when a certain resonance condition is met. A rippled bottom topography, if present, can act as a stationary wave and mediate weakly nonlinear interactions – a process known as 'Bragg resonance'. The conventional approach towards deriving the standard resonance conditions for weakly nonlinear wave triads, as well as Bragg scattering, fails to incorporate the effect of background velocity, especially of background shear. This is because these approaches are based on the potential flow theory, which dramatically simplifies the problem and allows one

to solve for the interfaces only. Since atmospheric and oceanic flows always have background velocity, it is imperative to account for the background flow in studying triads and Bragg resonances. We have taken a step forward in this direction by including a piecewise linear velocity profile, while still using the potential flow approximation. Although a piecewise linear velocity means a piecewise constant shear, which apparently cannot be dealt with using the potential flow theory, we use the result derived in Guha & Raj (2018) that the perturbed flow remains potential, even though the base flow has shear.

On incorporating background velocity, the resonance conditions for wave triads and Bragg scattering get strongly modified. Background velocity influences the resonance conditions in two ways: (i) by causing unequal Doppler shifts between the surface, pycnocline and the bottom (at least two of them), and (ii) by changing the intrinsic frequencies of the waves. We have explored various kinds of velocity fields – uniform, constant shear in the lower layer, constant shear in the upper layer and constant shear in both layers – to form a broad understanding of the effect of background velocity on triads and Bragg resonances. For Bragg resonance, even a uniform velocity field changes the resonance condition. In the absence of background shear, Bragg resonance only occurs when the two wave modes (the third 'wave' is the bottom ripple) lie on two distinct branches of the dispersion curve. However with shear (in the lower layer), we show that resonant triads appear even when the two wave modes lie on the same branch of the dispersion curve. In this regard interfacial modes are more susceptible than surface modes; modest Froude numbers are required in order to cause surface modes on the same branch to resonate; however, small Froude numbers are sufficient to do the same for the interfacial modes.

Using multiple scale analysis along with the Fredholm alternative, we have analytically obtained the equations governing the (slow) time evolution of the amplitudes of the waves forming both classical and Bragg triads up to $O(\epsilon^2)$. The formalism that we have developed has also been added to the higher-order spectral (HOS) method, a highly efficient and accurate numerical technique that can incorporate several triads up to any prescribed order of nonlinearity, which traditionally does not include background velocity. Using the 'modified' HOS we have numerically studied two problems on Bragg resonance: (i) the case when shear is present in the lower layer and leads to resonance between two wave modes lying on the same branch of the dispersion curve, and (ii) shear in the upper layer, which strongly affects the intrinsic frequencies. In the second case, we consider a bottom ripple consisting of three wavenumbers (chosen close to each other); a given incident wave resonantly generates only one wave, however two additional waves are generated via near-resonant interactions. Imposing the velocity field leads to change in the standard resonance condition and the wave generated in a near-resonant way may become resonant. This mechanism of near-resonant generation and effect of velocity field on resonance condition has been captured using the modified HOS method.

Acknowledgement

Appendix A. Derivation of dynamic boundary condition in the presence of a piecewise linear background shear

The inviscid Navier–Stokes equation within the bulk of a fluid of constant density ρ is

$$\rho \left[\boldsymbol{u}_{,t} + \tfrac{1}{2}\boldsymbol{\nabla}(\boldsymbol{u}\boldsymbol{\cdot}\boldsymbol{u}) - \boldsymbol{u}\times(\boldsymbol{\nabla}\times\boldsymbol{u}) \right] = -\boldsymbol{\nabla}p - \boldsymbol{\nabla}(\rho g z). \tag{A 1}$$

Using the fact that there is no base vorticity generation in the bulk, we have $\nabla \times \boldsymbol{u} = \nabla \times \bar{\boldsymbol{u}} = \Omega\hat{\jmath}$, where Ω is constant for each layer. In addition we use

$$\boldsymbol{u} \times (\Omega\hat{\jmath}) = \Omega\nabla\psi = \nabla(\Omega\psi). \tag{A 2}$$

Substituting (A 2) in (A 1) and removing the mean flow part, we are left with

$$\rho\left[\boldsymbol{u}'_{,t} + \tfrac{1}{2}\nabla(\boldsymbol{u}'\cdot\boldsymbol{u}') + \nabla(\bar{\boldsymbol{u}}\cdot\boldsymbol{u}') - \nabla(\Omega\psi')\right] = -\nabla p' - \nabla(\rho g\eta). \tag{A 3}$$

Since the perturbed flow is irrotational, we introduce $\boldsymbol{u}' = \nabla\phi'$. Moreover, since the density is constant within each layer, we obtain

$$\nabla\left[\rho\left(\phi'_{,t} + \tfrac{1}{2}\nabla\phi'\cdot\nabla\phi' + \bar{\boldsymbol{u}}\cdot\nabla\phi' - \Omega\psi' + g\eta\right) + p'\right] = 0. \tag{A 4}$$

Since this is true for any arbitrary curve inside the domain, we have on integration

$$\rho\left(\phi'_{,t} + \tfrac{1}{2}\nabla\phi'\cdot\nabla\phi' + \bar{\boldsymbol{u}}\cdot\nabla\phi' - \Omega\psi' + g\eta\right) + p' = c, \tag{A 5}$$

where c is an arbitrary function of time, which turns out to be zero in order to satisfy the unperturbed far-field condition. Thus, equating the pressure just above and just below the interface $z = \eta(x, t)$, at which the base flow velocity is $\bar{\boldsymbol{u}} = U\hat{\imath}$, we obtain

$$\rho_1\left(\phi'_{1,t} + \tfrac{1}{2}\nabla\phi'_1\cdot\nabla\phi'_1 + U\hat{\imath}\cdot\nabla\phi'_1 - \Omega_1\psi' + g\eta\right)$$
$$= \rho_2\left(\phi'_{2,t} + \tfrac{1}{2}\nabla\phi'_2\cdot\nabla\phi'_2 + U\hat{\imath}\cdot\nabla\phi'_2 - \Omega_2\psi' + g\eta\right). \tag{A 6}$$

Dropping the primes, we get

$$\rho_1\left[\phi_{1,t} + \tfrac{1}{2}(\phi_{1,x}^2 + \phi_{1,z}^2) + U\phi_{1,x} - \Omega_1\psi_1 + g\eta\right]$$
$$= \rho_2\left[\phi_{2,t} + \tfrac{1}{2}(\phi_{2,x}^2 + \phi_{2,z}^2) + U\phi_{2,x} - \Omega_2\psi_2 + g\eta\right]. \tag{A 7}$$

Appendix B. Relevant coefficients

The coefficients $\boldsymbol{n}_j$ are same for the case of wave triad interaction and the case of Bragg resonance. They are simply the null vector of the transpose of the matrix $\boldsymbol{D}(k_j, \omega_j)$. The coefficients of time derivatives of $O(\epsilon)$ terms, i.e. the vector $\boldsymbol{r}_j$ also remains the same both for wave triad interaction and Bragg resonance.

The components of the vector $\boldsymbol{r}_j$ are

$$\left.\begin{array}{l}
r_j(1) = 1, \\
r_j(2) = T_j, \\
r_j(3) = T_j, \\
r_j(4) = -iQ_j, \\
r_j(5) = -\dfrac{i}{k_j}\left[T_j(\omega_j - k_jU_l)\left(\tanh k_jh_u + \dfrac{1}{\tanh k_jh_l}\right) + \dfrac{Q_j}{\cosh k_jh_u}\right], \\
r_j(6) = 0.
\end{array}\right\} \tag{B 1}$$

$$T_j = \frac{\cosh(k_jh_u)[(\omega_j - U_uk_j)^2 + (\omega_j - U_uk_j)\Omega_u\tanh(k_jh_u) - gk_j\tanh(k_jh_u)]}{(\omega_j - U_lk_j)(\omega_j - U_uk_j)}, \tag{B 2}$$

$$Q_j = \frac{\Omega_u}{k_j} + \frac{g}{U_u k_j - \omega_j}. \tag{B 3}$$

For the case of wave triad interaction the coefficients of $\boldsymbol{v}_1$ are as follows:

$$v_1(1) = -\mathrm{i}g k_1 \left(\frac{\Omega_u}{g} + \frac{k_2}{U_u k_2 - \omega_2} + \frac{k_3}{U_u k_3 - \omega_3} \right), \tag{B 4}$$

$$v_1(2) = -\mathrm{i}k_1 \left[\frac{k_2 T_3 Q_2}{\cosh k_2 h_u} + \frac{k_3 T_2 Q_3}{\cosh k_3 h_u} + T_2 T_3 \left(\frac{\omega_2 - U_l k_2}{\tanh k_2 h_u} + \frac{\omega_3 - U_l k_3}{\tanh k_3 h_u} - \Omega_u \right) \right], \tag{B 5}$$

$$v_1(3) = -\mathrm{i}T_2 T_3 k_1 \left(\frac{k_2 U_l - \omega_2}{\tanh k_2 h_l} + \frac{k_3 U_l - \omega_3}{\tanh k_3 h_l} - \Omega_l \right), \tag{B 6}$$

$$
\begin{aligned}
v_1(4) = {} & \frac{T_2(U_l k_2 - \omega_2)}{\cosh k_2 h_l}(k_2 U_u - \omega_2 + k_3 Q_3 \tanh k_3 h_l) \\
& + \frac{T_3(U_l k_3 - \omega_3)}{\cosh k_3 h_l}(k_3 U_u - \omega_3 + k_2 Q_3 \tanh k_3 h_l) \\
& + (U_u k_3 - \omega_3)k_3 Q_3 \tanh k_2 h_u + (U_u k_2 - \omega_2)k_2 Q_2 \tanh k_2 h_u \\
& - Q_2 Q_3 k_2 k_3 (1 - \tanh k_2 h_u \tanh k_3 h_u) + \frac{T_2 T_3(\omega_2 - U_l k_2)(\omega_3 - U_l k_3)}{\cosh k_2 h_u \cosh k_3 h_l},
\end{aligned} \tag{B 7}
$$

$$
\begin{aligned}
v_1(5) = {} & T_2 T_3(R-1)[(k_3 U_l - \omega_3)^2 + (k_2 U_l - \omega_2)^2 + (k_2 U_l - \omega_2)(k_3 U_l - \omega_3)] \\
& - \frac{R k_2 k_3 Q_2 Q_3}{\cosh k_2 h_u \cosh k_3 h_u} + R k_2 T_3 Q_2 \frac{(k_3 U_l - \omega_3) \tanh k_3 h_u}{\cosh k_2 h_u} \\
& + R k_3 T_2 Q_3 \frac{(k_2 U_l - \omega_2) \tanh k_2 h_u}{\cosh k_3 h_u} - T_2 T_3(k_2 U_l - \omega_2)(k_3 U_l - \omega_3) \\
& \times \left(R \tanh k_2 h_u \tanh k_3 h_u - \frac{1}{\tanh k_2 h_l \tanh k_3 h_u} \right),
\end{aligned} \tag{B 8}
$$

$$v_1(6) = 0. \tag{B 9}$$

Similarly, the terms of the vectors $\boldsymbol{v}_2$ and $\boldsymbol{v}_3$ can be obtained by changing the indices in a cyclic order, i.e. the substitution $\{1 \to 2, 2 \to 3, 3 \to 1\}$ in the above equations.

For the case of Bragg resonance, where $k_3 \equiv k_b = k_1 + k_2$ and $\omega_3 = \omega_b = 0$ we have two cases,

Case 1: $U_b = 0$.

$$
\left.
\begin{aligned}
v_1(1) = v_1(2) &= v_1(3) = v_1(4) = v_1(5) = 0, \\
v_1(6) &= \mathrm{i}\frac{k_1(\omega_2 - U_l k_2)T_2}{\sinh k_2 h_u}; \\
v_2(1) = v_2(2) &= v_2(3) = v_2(4) = v_2(5) = 0, \\
v_2(6) &= \mathrm{i}\frac{k_2(\omega_1 - U_l k_1)T_1}{\sinh k_1 h_u}.
\end{aligned}
\right\} \tag{B 10}
$$

The vector $\boldsymbol{r}_j$ remains the same as before.

Case 2: $U_b \neq 0$.

In this case, the bottom boundary condition would be inhomogeneous. This will mean that there will exists a time-independent particular solution of the system at $O(\epsilon)$ having

$$
\left.
\begin{aligned}
\hat{\eta}_u &= -\frac{U_u U_b U_l^2 k_b^6}{\det(\boldsymbol{D})(0, k_b) \cosh k_b h_u \cosh^2 k_b h_l} \hat{\eta}_b \equiv X_{b1} \hat{\eta}_b, \\[2mm]
\hat{\eta}_l &= -\frac{U_b U_l k_b^5 (U_u^2 k_b \cosh k_b h_u - (\Omega_u U_u + g) \sinh k_b h_u)}{\det(\boldsymbol{D})(0, k_b) \cosh k_b h_u \cosh^2 k_b h_l} \hat{\eta}_b \equiv X_{b2} \hat{\eta}_b, \\[2mm]
\hat{A} &= -\mathrm{i} \frac{U_b U_l^2 k_b^5 (\Omega_u U_u + g)}{\det(\boldsymbol{D})(0, k_b) \cosh k_b h_u \cosh^2 k_b h_l} \hat{\eta}_b \equiv \mathrm{i} X_{b3} \hat{\eta}_b, \\[2mm]
\hat{B} &= -\mathrm{i} \frac{U_b U_l^2 k_b^5 (\cosh k_b h_u U_u^2 k_b - \sinh k_b h_u (\Omega_u U_u + g))}{\det(\boldsymbol{D})(0, k_b) \cosh k_b h_u \cosh^2 k_b h_l} \hat{\eta}_b \equiv \mathrm{i} X_{b4} \hat{\eta}_b, \\[2mm]
\hat{C} &= -\mathrm{i} \frac{U_b (k_b^6 U_u^2 U_l^2 + \det(\boldsymbol{D})(0, k_b) \cosh^3 k_b h_l - k_b^5 U_l^2 (\Omega_u U_u + g) \tanh k_b h_u)}{\det(\boldsymbol{D})(0, k_b) \cosh k_b h_l \sinh k_b h_l} \hat{\eta}_b \equiv \mathrm{i} X_{b5} \hat{\eta}_b, \\[2mm]
\hat{D} &= \mathrm{i} U_b \cosh k_b h_l \hat{\eta}_b \equiv \mathrm{i} X_{b6} \hat{\eta}_b.
\end{aligned}
\right\}
\tag{B 11}
$$

The coefficients $v_2(1), v_2(2), v_2(3), v_2(4), v_2(5)$ may not be zero if $U_b \neq 0$ and will be given as:

$$
v_2(1) = -\mathrm{i} k_2 (k_b Q_1 X_{b1} + k_b X_{b3} + \Omega_u X_{b1}),
\tag{B 12}
$$

$$
\begin{aligned}
v_2(2) &= \mathrm{i} k_2 \left(\frac{X_{b2}(T_1(k_1 U_l - \omega_1) \sinh k_1 h_u - k_1 Q_1)}{\cosh k_1 h_u} \right. \\
&\quad \left. + \frac{T_1(-X_{b4} \sinh k_3 h_u + X_{b3}) k_b}{\cosh k_b h_u} + \Omega_u T_1 X_{b_2} \right),
\end{aligned}
\tag{B 13}
$$

$$
v_2(3) = -\mathrm{i} k_2 T_1 \left(\frac{X_{b2}(k_1 U_l - \omega_1)}{\tanh k_1 h_l} - X_{b6} k_1 \tanh k_1 h_l + k_b X_{b5} - \Omega_l X_{b2} \right),
\tag{B 14}
$$

$$
\begin{aligned}
v_2(4) &= T_1 X_{b1} \frac{(k_1 U_l - \omega_1)}{k_1 U_u - \omega_1} \cosh k_1 h_u + k_1 Q_1 X_{b1}(k_1 U_u - \omega_1) \tanh k_1 h_u \\
&\quad - k_b \left(X_{b3} \tanh k_b h_u + \frac{X_{b4}}{\cosh k_b h_u} \right) \left(\frac{T_1(k_1 U_l - \omega_1)}{\cosh k_1 h_u} - k_b U_u \right) \\
&\quad - Q_1 k_1 X_{b3} k_b (\tanh k_1 h_u \tanh k_b h_u + 1) - \frac{Q_1 k_1 X_{b4} k_b \tanh k_1 h_u}{\cosh k_b h_u},
\end{aligned}
\tag{B 15}
$$

$$
\begin{aligned}
v_2(5) &= T_1 \left(\frac{\Omega_l X_{b6} k_b}{\coth k_b h_l} - \frac{U_l X_{b5} k_b^2}{\coth k_b h_l} + R U_l X_{b4} k_b^2 - X_{b6} k_1 U_l k_b \right) \\
&\quad + T_1 (k_1 U_l - \omega_1) \left[-\frac{R k_b X_{b4}}{\coth k_1 h_u \coth k_b h_u} + (k_1 U_l - \omega_1) X_{b2}(R - 1) \right. \\
&\quad \left. + X_{b6}(k_1 + k_b) - R X_{b4} k_b + \frac{k_b \tanh k_1 h_u R X_{b3}}{\cosh k_b h_u} + \frac{k_b X_{b5}}{\tanh k_1 h_l} + \frac{k_b X_{b5}}{\coth k_b h_l} \right] \\
&\quad + R k_1 k_b Q_1 \frac{X_{b4} \sinh k_b h_u - X_{b3}}{\cosh k_1 h_u \cosh k_b h_u} + \frac{\Omega_l k_b T_1}{\sinh k_1 h_l} \left(\frac{1}{\cosh k_1 h_l} - \cosh k_1 h_l \right),
\end{aligned}
\tag{B 16}
$$

$$
v_2(6) = \mathrm{i} \frac{k_2(\omega_1 - U_l k_1) T_1}{\sinh k_1 h_u}.
\tag{B 17}
$$

The coefficients $v_1(1), v_1(2), v_1(3), v_1(4), v_1(5)$ will be given by swapping k_2 and k_1 in the above equations.

Appendix C. Boundary conditions

C.1. *Dirichlet boundary conditions*

We expand the velocity potential as a perturbation series up to an order '(m)'. So, from (5.11) we have,

$$\phi^S(x, t) = \sum_{m=1}^{M} \sum_{k=0}^{M-m} \frac{\eta_u^k}{k!} \frac{\partial^k}{\partial z^k} \phi_u^{(m)}(x, z, t)\bigg|_{z=0}. \tag{C 1}$$

Collecting the terms of leading order, that is terms of $O(\epsilon)$, we have,

$$\phi_u(x, 0, t) = \phi^S(x, t). \tag{C 2}$$

Further, collecting the terms of $O(\epsilon^m)$ from (5.11), we have,

$$\left.\begin{aligned}
\sum_{k=0}^{m-1} \frac{\eta_u^k}{k!} \frac{\partial^k}{\partial z^k} \phi_u^{(m-k)}(x, z, t)\bigg|_{z=0} &= 0, \\
\Rightarrow \sum_{k=1}^{m-1} \frac{\eta_u^k}{k!} \frac{\partial^k}{\partial z^k} \phi_u^{(m-k)}(x, z, t)\bigg|_{z=0} &+ \phi_u^{(m)}(x, z, t)|_{z=0} = 0, \\
\Rightarrow \phi_u^{(m)}(x, 0, t) &= -\sum_{k=1}^{m-1} \frac{\eta_u^k}{k!} \frac{\partial^k}{\partial z^k} \phi_u^{(m-k)}(x, z, t)\bigg|_{z=0}.
\end{aligned}\right\} \tag{C 3}$$

So, combining the boundary conditions at every order, we can write,

$$\phi_u^{(m)}(x, 0, t) = f_u^{(m)}, \tag{C 4}$$

where

$$f_u^{(1)} = \phi^S, \tag{C 5}$$

$$f_u^{(m)} = -\sum_{k=1}^{m-1} \frac{\eta_u^k}{k!} \frac{\partial^k}{\partial z^k} \phi_u^{(m-k)}(x, z, t)\bigg|_{z=0}. \tag{C 6}$$

In a very similar way, we can derive the Dirichlet boundary condition at the pycnocline.

C.2. *Neumann boundary condition*

Firstly, we subtract the two kinematic boundary conditions at the pycnocline to get rid of the time derivative, and obtain

$$\varphi_{,z}(x, z, t) = \eta_{l,x}\varphi_{,x}(x, z, t) + \eta_l\eta_{l,x}(\Omega_u - \Omega_l) \quad z = -h_u + \eta_l. \tag{C 7}$$

Note, that we have expanded the base velocity U in a Taylor series about the mean surface. Here, $\varphi(x, z, t) \equiv \phi_u(x, z, t) - \phi_l(x, z, t)$. We expand $\varphi(x, z, t)$ in a Taylor expansion about the mean height of the interface to get

$$\varphi(x, -h_u + \eta_l, t) = \sum_{m=1}^{M} \sum_{k=0}^{M-m} \frac{\eta_l^k}{k!} \frac{\partial^k}{\partial z^k} \varphi^{(m)}(x, z, t)\bigg|_{z=-h_u}. \tag{C 8}$$

Substituting this in the (C 7), while keeping aside the term $\eta_l \eta_{l,x}(\Omega_u - \Omega_l)$ for now, we have,

$$\sum_{m=1}^{M} \sum_{k=0}^{M-m} \frac{\eta_l^k}{k!} \frac{\partial^k}{\partial z^k} \varphi_{,z}^{(m)}(x, z, t) \bigg|_{z=-h_u} = \frac{\partial \eta_l}{\partial x} \sum_{m=1}^{M} \sum_{k=0}^{M-m} \frac{\eta_l^k}{k!} \frac{\partial^k}{\partial z^k} \varphi_{,x}^{(m)}(x, z, t) \bigg|_{z=-h_u}. \tag{C 9}$$

Again, collecting the terms of $O(\epsilon^m)$ from the above equation we have

$$\left.\begin{aligned} \sum_{k=0}^{m-1} \frac{\eta_l^k}{k!} \frac{\partial^k}{\partial z^k} \varphi_{,z}^{(m-k)} \bigg|_{z=-h_u} &= \frac{\partial \eta_l}{\partial x} \sum_{k=1}^{m-1} \frac{\eta_l^{k-1}}{(k-1)!} \frac{\partial^{k-1}}{\partial z^{k-1}} \varphi_{,x}^{(m-k)} \bigg|_{z=-h_u} \\ \Rightarrow \sum_{k=1}^{m-1} \frac{\eta_l^k}{k!} \frac{\partial^k}{\partial z^k} \varphi_{,z}^{(m-k)} \bigg|_{z=-h_u} + \varphi_{,z}^{(m)}|_{z=-h_u} &= \sum_{k=1}^{m-1} \frac{\partial \eta_l}{\partial x} \frac{\eta_l^{k-1}}{(k-1)!} \frac{\partial^{k-1}}{\partial z^{k-1}} \varphi_{,x}^{(m-k)} \bigg|_{z=-h_u}. \end{aligned}\right\} \tag{C 10}$$

Now, using the continuity equation we have,

$$\left.\begin{aligned} \frac{\partial^2 \phi_u}{\partial z^2} &= -\frac{\partial^2 \phi_u}{\partial x^2} \\ \Rightarrow \frac{\partial^k \phi_{u,z}}{\partial z^k} &= -\frac{\partial^{k-1}}{\partial z^{k-1}} \phi_{u,xx} \quad \text{for } k > 0. \end{aligned}\right\} \tag{C 11}$$

Similarly, we have,

$$\frac{\partial^k \phi_{l,z}}{\partial z^k} = -\frac{\partial^{k-1}}{\partial z^{k-1}} \phi_{l,xx}. \tag{C 12}$$

Subtracting the above two equations, we obtain,

$$\frac{\partial^k \varphi_{,z}}{\partial z^k} = -\frac{\partial^{k-1}}{\partial z^{k-1}} \varphi_{,xx}. \tag{C 13}$$

Now using the above result in (C 10), we have,

$$-\sum_{k=1}^{m-1} \frac{\eta_l^k}{k!} \frac{\partial^{k-1}}{\partial z^{k-1}} \varphi_{,xx}^{(m-k)} \bigg|_{z=-h_u} + \varphi_{,z}^{(m)}|_{z=-h_u} = \sum_{k=1}^{m-1} \frac{\partial \eta_l}{\partial x} \frac{\eta_l^{k-1}}{(k-1)!} \frac{\partial^{k-1}}{\partial z^{k-1}} \varphi_{,x}^{(m-k)} \bigg|_{z=-h_u}. \tag{C 14}$$

Rearranging the terms, we have,

$$\varphi_{,z}^{(m)}|_{z=-h_u} = \sum_{k=1}^{m-1} \frac{\partial^{k-1}}{\partial z^{k-1}} \left[\frac{\eta_l^{k-1}}{(k-1)!} \frac{\partial \eta_l}{\partial x} \varphi_{,x}^{(m-k)} + \frac{\eta_l^k}{k!} \varphi_{,xx}^{(m-k)} \right]_{z=-h_u}, \tag{C 15}$$

$$\Rightarrow \varphi_{,z}^{(m)}|_{z=-h_u} = \sum_{k=1}^{m-1} \frac{\partial^{k-1}}{\partial z^{k-1}} \frac{\partial}{\partial x} \left[\frac{\eta_l^k}{k!} \varphi_x^{(m-k)} \right]_{z=-h_u}, \tag{C 16}$$

$$\Rightarrow \varphi_{,z}^{(m)}|_{z=-h_u} = \sum_{k=1}^{m-1} \frac{\partial}{\partial x} \left[\frac{\eta_l^k}{k!} \frac{\partial^{k-1}}{\partial z^{k-1}} \varphi_x^{(m-k)} \right]_{z=-h_u}. \tag{C 17}$$

Now, we include the term $\eta_l \eta_{l,x}(\Omega_u - \Omega_l)$, the effect of which will be only in the $O(\epsilon^2)$ terms. So, finally we have

$$\varphi_{,z}^{(m)}(x, -h_u, t) = f_{l2}^{(m)}, \tag{C 18}$$

where

$$f_{l2}^{(1)} = 0, \tag{C 19}$$

$$f_{l2}^{(2)} = \frac{\partial}{\partial x}[\eta_l \varphi_{,x}^{(1)}(x, z, t)|_{z=-h_u}] + \eta_l \eta_{l,x}(\Omega_u - \Omega_l), \tag{C 20}$$

$$f_{l2}^{(m)} = \sum_{k=1}^{m-1} \frac{\partial}{\partial x} \left[\frac{\eta_l^k}{k!} \frac{\partial^{k-1}}{\partial z^{k-1}} \varphi_{,x}^{(m-k)}(x, z, t) \bigg|_{z=-h_u} \right]. \tag{C 21}$$

At $O(\epsilon)$ in a similar way we can derive the bottom boundary condition, which is also a Neumann boundary condition.

REFERENCES

ALAM, M.-R. 2012 Broadband cloaking in stratified seas. *Phys. Rev. Lett.* **108** (8), 084502.

ALAM, M.-R., LIU, Y. & YUE, D. K. P. 2009*a* Bragg resonance of waves in a two-layer fluid propagating over bottom ripples. Part I. Perturbation analysis. *J. Fluid Mech.* **624**, 191–224.

ALAM, M.-R., LIU, Y. & YUE, D. K. P. 2009*b* Bragg resonance of waves in a two-layer fluid propagating over bottom ripples. Part II. Numerical simulation. *J. Fluid Mech.* **624**, 225–253.

BAKER, G. R., MEIRON, D. I. & ORSZAG, S. A. 1982 Generalized vortex methods for free-surface flow problems. *J. Fluid Mech.* **123**, 477–501.

BALL, F. K. 1964 Energy transfer between external and internal gravity waves. *J. Fluid Mech.* **19**, 465–478.

CAIRNS, R. A. 1979 The role of negative energy waves in some instabilities of parallel flows. *J. Fluid Mech.* **92**, 1–14.

CRAIK, A. D. D. 1988 *Wave Interactions and Fluid Flows*. Cambridge University Press.

DAVIES, A .G. 1982 The reflection of wave energy by undulations on the seabed. *Dyn. Atmos. Oceans* **6** (4), 207–232.

DOMMERMUTH, D. G. & YUE, D. K. P. 1987 A high-order spectral method for the study of nonlinear gravity waves. *J. Fluid Mech.* **184**, 267–288.

DRAZIN, P. G. 2002 *Introduction to Hydrodynamic Stability*. Cambridge University Press.

DRIVAS, T. D. & WUNSCH, S. 2016 Triad resonance between gravity and vorticity waves in vertical shear. *Ocean Model.* **103**, 87–97.

ELGAR, S., RAUBENHEIMER, B. & HERBERS, T. H. C. 2003 Bragg reflection of ocean waves from sandbars. *Geophys. Res. Lett.* **30** (1), 1016.

GEYER, W. R., RALSTON, D. K. & HOLLEMAN, R. C. 2017 Hydraulics and mixing in a laterally divergent channel of a highly stratified estuary. *J. Geophys. Res.* **122** (6), 4743–4760.

GUHA, A. & LAWRENCE, G. A. 2014 A wave interaction approach to studying non-modal homogeneous and stratified shear instabilities. *J. Fluid Mech.* **755**, 336–364.

GUHA, A. & RAJ, R. 2018 On the inertial effects of density variation in stratified shear flows. *Phys. Fluids* **30**, 126603.

HARNIK, N., HEIFETZ, E., UMURHAN, O. M. & LOTT, F. 2008 A buoyancy–vorticity wave interaction approach to stratified shear flow. *J. Atmos. Sci.* **65** (8), 2615–2630.

HEATHERSHAW, A. D. & DAVIES, A. G. 1985 Resonant wave reflection by transverse bedforms and its relation to beaches and offshore bars. *Mar. Geol.* **62** (3–4), 321–338.

HILL, D. F. & FODA, M. A. 1996 Subharmonic resonance of short internal standing waves by progressive surface waves. *J. Fluid Mech.* **321**, 217–233.

KIRBY, J. T. 1986 A general wave equation for waves over rippled beds. *J. Fluid Mech.* **162**, 171–186.

KIRBY, J. T. 1988 Current effects on resonant reflection of surface water waves by sand bars. *J. Fluid Mech.* **186**, 501–520.

MCHUGH, J. P. 1992 The stability of capillary-gravity waves on flow over a wavy bottom. *Wave Motion* **16** (1), 23–31.

MEI, C. C. 1985 Resonant reflection of surface water waves by periodic sandbars. *J. Fluid Mech.* **152**, 315–335.

PEREGRINE, D. H. 1976 Interaction of water waves and currents. *Adv. Appl. Maths.* **16**, 9–117.

RAJ, R. & GUHA, A. 2018 Explosive instability due to flow over a rippled bottom. Preprint, arXiv:1809.07507.

SHETE, M. H. & GUHA, A. 2018 Effect of free surface on submerged stratified shear instabilities. *J. Fluid Mech.* **843**, 98–125.

VALLIS, G. K. 2017 *Atmospheric and Oceanic Fluid Dynamics*. Cambridge University Press.

WEN, F. 1995 Resonant generation of internal waves on the soft sea bed by a surface water wave. *Phys. Fluids* **7**, 1915–1922.